

Role of special crosslinks in structure formation of DNA polymer.

Tejal Agarwal¹, G.P. Manjunath², Farhat Habib³, Pavna Lakshmi¹, Apratim Chatterji^{1,4*}

¹ *IISER-Pune, 900 NCL Innovation Park, Dr. Homi Bhaba Road, Pune-411008, India.*

² *IISER Mohali, Knowledge city, Sector 81, SAS Nagar, Manauli-140306, India.*

³ *Innobi, Cessna Business Park, Outer Ring Road, Bangalore-560103, India.*

⁴ *Center for Energy Science, IISER-Pune, Dr. Homi Bhaba Road, Pune-411008, India.*

(Dated: June 5, 2019)

Using data from contact maps of the DNA-polymer of *E. Coli* (at kilo base pair resolution) as an input to our model, we introduce cross-links between monomers in a bead-spring model of a ring polymer at very specific points along the chain. By suitable Monte Carlo Simulations we show that the presence of these cross-links lead to a specific architecture and organization of the chain at large (micron) length scales of the DNA. We also investigate the structure of a ring polymer with an equal number of cross-links at random positions along the chain. We find that though the polymer does get organized at the large length scales, the nature of organization is quite different from the organization observed with cross links at specific biologically determined positions. We used the contact map of e-coli bacteria which has around 4.6 million base pairs in a single chromosome. In our coarse grained flexible ring polymer model we used 4600 monomer beads and observe that around 80 cross links are enough to induce large scale organization of the molecule accounting for statistical fluctuations induced by thermal energy. The length of a DNA chain of a even simple bacterial cell such as ecoli is much longer than typical proteins, hence we avoided methods used to tackle protein folding problems. We define new suitable quantities to identify large scale structure of a polymer chain with a few cross-links.

PACS numbers: 87.15.ak,82.35.Lr,82.35.Pq,87.16.Sr,61.25.hp

I. INTRODUCTION

The organization of chromatin at mesoscopic length ($> 30nm$) scales has been a topic of intense research in this decade [1–21], specially after the work of Liebermann Aiden et. al. [2] where the authors mapped out the spatial proximity maps of DNA segments of human genome (each segment of length 1 Mega Base Pair of nucleic acid) inside nucleus using a technique called Hi-C: high-throughput sequencing. The experimental studies provide a *contact map* of DNA segments [2, 4–6, 22–24]. A contact map is a color map which shows which DNA segments, numbered $i = 1, 2, 3 \dots N_D$ are spatially close to other DNA segments j ($j = 1, \dots, N_D$) with high/low frequency. The question is whether with this information, can one predict the spatial organization of the entire DNA chain and then identify the biological consequences.

The physics approach is of course to consider chromatin as a polymer chain, and the chromatin within the nucleus as a collapsed polymer globule [3, 7, 14, 16, 17, 25–38]. It has also been fairly established that the organization of chromatin inside the nucleus is a fractal globule rather than an equilibrium globule [25, 26]. Before going further, a clarification of various terms and specification of different length scales are as follows: A double stranded DNA (ds-DNA) helix made by combinations of base pairs (BP) of 4 nucleic acids (A,T,G,C) has a width of 10 Å, a helical pitch of 34 Å with 11 BP

in a pitch. Each BP is of size 3.3 Å. Each of the human cells has 46 ds-DNA chains, and the total length of DNA in each cell is about 2 meters if the chains were arranged back to back in a straight line. These chains are packed in a nucleus typically of volume $10\mu^3$. To achieve this, DNA chains form a hierarchy of coiled structures. For example ds-DNA wrap around histone proteins to form higher order structure called nucleosome. These nucleosome beads are joined together by ds-DNA segments whose length can vary from 10 to 100 BPs. The chain of nucleosome beads form a 30 nm fiber with a characteristic width of 30 nm [39]. How the 30 nm fiber, also known as chromatin, is further packed into higher order structures not clearly known. If there exists a well defined structure and organization of DNA at large length scales at all is a topic of intense investigation from perspectives of soft matter polymer physics as well as biology. Polymer-physicists and biologists often collaborate and work together to investigate the possible schemes of organization at *large* length scales. The *large* length scales of ds-DNA in question are $100nm-\mu$, with DNA-segments constituting of kilo to mega BPs. Our work aims to elucidate the structure of chromatin at this length scale and above. The fully compacted DNA chain inside the nucleus is referred as a chromosome. A human cell has 23 pairs of chromosomes [39].

Often, for a physicist it is easier and relevant to work with simpler systems, e.g. DNA of bacteria such as *Escherichia coli* (*E. coli*). Bacterial cells have no nucleus, the number of chromosomes is typically 1 or 2 per cell, and the DNA-polymers are much shorter. Bacterial DNA is also expected to be organized, instead of histones they have other histone-like proteins, and they have other suit-

* apratim@iiserpune.ac.in

able CTCF proteins which may bind two sections of the DNA segments together [6].

Most of the research focus on structure and organization of the chromatin during interphase stage [7, 10, 15, 25, 26, 40]: the stage of cell cycle when cell does not divide into daughter cells. During this stage, different chromosomes do not form an entangled melt of chromatin polymer (to borrow a polymer physics terminology), but instead are found at a specific locations within the nucleus surrounded by fairly well defined neighbouring chromatin chains. For example for the case of humans number 5 chromosome is likely to be found near the nucleus wall and is typically chromosome 1,2,3. Thus chromosomes are found at relatively well defined locations within the cell nucleus and this organization within nucleus is called Chromosomal Territories [2, 10, 25].

A related question is, whether there is some organization within each individual chromosome, and the contact map of a single chromosome clearly indicates such organization. From the data of contact map we observe that some DNA chain segments have much higher spatial association with other chain segments which are close along the chain contour and show up as the presence of so called Topologically Associated Domains (TADs) [2, 5, 6, 22]. It would be important to stress that an actual chromatin chain within a nucleus is not just a long polymer chain with monomers but also there are various proteins and enzymes doing various functions including insulator Binding Proteins [6] which attach two specific segments of DNA chain together and enzyme topoisomerase which allow chains to pass through each other and release topological constraints by suitably cutting and rejoining chains [27].

As we mention earlier the big question is: how do the individual chromatin fiber arrange itself at large length-scales and if one can possibly predict the structure of the chain from the knowledge of contact maps and TADs? Using principles of polymer physics, a few researchers have focussed on how and why the TADs are formed [1, 7, 10, 13, 25, 26]. The current understanding is that neighbouring segments of chromatin get locally collapsed to form *unentangled* crumpled sections of the globule, so that within a section of the globule there are many contacts between the DNA-segments. Thus the entire globule consists of many collapsed sections of the DNA in contact with each other: this structure is called the fractal globule. A consequence is that there are large number of contacts within a section of the chain, these then show up as TADs in the contact map. In addition to these there are also high frequency of contacts between the segments which are far separated along the contour of the chains.

It has been established that the organization of a DNA chain is very different from entangled globule of semi-dilute polymer which is referred as an equilibrium globule in this literature. In equilibrium globule the distance $R(s)$ between two points along the chain separated by contour length s follows the scaling law $R(s) \sim s^{1/3}$ for

$s < N^{2/3}$ and $R(s)$ is independent of s for $s > N^{2/3}$, in contrast to the fractal globule state of a polymer where $R(s) \sim s^{1/3}$. Note however in both cases the radius of the globule R_g scales as $R_g \sim N^{1/3}$. Furthermore the contact probability: the probability of contact between different segments of the chain scales differently. For equilibrium globule $P_c(s) \sim s^{-3/2}$ for $s < N^{2/3}$; $P_c(s) \sim \text{constant}$ for $s > N^{2/3}$ whereas for fractal globule $P_c(s) \sim s^{-1}$ showing that there is a much higher probability of contacts between segments which are close to each other [26]. The fractal globule is not a thermodynamically equilibrium state of polymer, and anyway life time of a cell is much smaller than the relaxation time of DNA polymers, so that DNA does not get a chance to relax to equilibrium. Of course the cell is not in the thermodynamical equilibrium as there are many biologically driven active processes going on inside the cell.

We propose a different approach from the studies mentioned above, putting in minimal biological inputs in the modelling of the DNA-chain but still using mesoscopic coarse grained models. This is similar in spirit to the methods used by [17, 32, 41, 42] while analyzing the structural organization of the chromatin. We suggest the hypothesis that crosslinks above a critical number and at special locations along the chain are instrumental in giving shape and structure to the chromatin at large length scales. We choose a simpler system: a bead spring flexible polymer model of e-coli, a bacterial DNA without any nucleus wall and with a single chromosome to test our hypothesis. In the first step we intentionally avoid the study of higher organism with many chromatin chains which themselves form chromosomal territory within nucleus. Using experimental data [22] about the location of segments along the chain which are found to be in spatial proximity with specific other segments with much higher frequency than other pairs (this could arise from DNA-binding proteins or other reasons), we introduce extra constraints as cross-links (CLs) between two specific monomer beads of our model polymer-chain of DNA. These pair of monomer-beads, each representing different segments of the DNA, could be well separated along the length of the chain. The extra cross-links are modelled by adding an harmonic potential between a pair of specific monomers.

We start our Monte Carlo (MC) simulation from 9 independent initial configuration of monomers but with the same set of biologically determined locations of cross-links in each case. We then allow the chains to relax in 9 independent MC runs. We observe that the DNA polymer relaxes to almost the same “structure” within statistical fluctuations in each case. We thus confirm our hypothesis that having CLs at specific biologically determined locations and above a critical number do lead to the spatial organization of the chromosome. To achieve this, we had to come up with different structural quantities akin to pair correlation function $g(r)$ from which we could deduce the overall organization of the DNA-polymer molecule. In contrast to the studies with bio-

logically determined position of CLs, when we carry out similar 9 sets of MC runs using ring polymers of identical length but with CLs at randomly chosen locations along the chain, we observe different nature of organization of the DNA polymer. Our hypothesis can be further established by testing it on more bacterial chromosomes and may be in chromosomes of higher organisms in the future. We also have results to establish that DNA-polymer of the the bacteria *Caulobacter Crescentus* (*C. Crescentus*) gets organized into a particular structure due to the presence of CLs in appropriate locations suitable for *C. Crescentus*. This will be reported elsewhere. *C. Crescentus* has around 4 million BPs in its DNA. We re-emphasize that we are aiming to investigate the organized structure of the DNA molecule at a length scale of 100 nm or more, i.e. much larger than the double helix structure (1 nm length scale) or the scale of DNA architecture organized by the DNA binding proteins (150 base pairs with a length scale of 10 nm).

The chromosome of bacteria *Escherichia Coli* (*E. Coli*) is a ring with 4642 kilo BPs: to that end our model of *E. Coli* chromosome is a ring polymer with 4642 monomer beads linked together along the chain. Thus we consider a monomer bead of our model to be 10^3 base pairs. Note that the Kuhn length of DNA is $1000 \text{ \AA} \equiv 300 \text{ BPs}$. At the length scales under consideration it is valid to consider the DNA as a flexible polymer chain. Moreover, the bacterial DNAs under consideration is a ring polymer. Polymer rings get less entangled than linear polymers [43]. Information of any pair of monomers i and j to be close to each other have been extracted from the contact maps (discussed further in the Appendix). We emphasize and clarify that the observation of particular monomers to be in proximity with high frequency is incorporated in our coarse-grained model of DNA-polymer as *permanent* cross-links between particular monomers i and j . The primary hurdle is then to identify the statistical quantities which can resolve the structure and organization of a DNA polymer, especially when it is known that polymers have random and rapidly changing conformations due to thermal fluctuations. We have come up with various quantities using which we can reliably conclude whether a set of (biologically determined) constraints leads to a most probable organization of the DNA molecule, we discuss these later in this paper.

The organization of the manuscript is as follows: the next section, viz., section II discusses the computational method by which we generate conformations using which we calculate statistical quantities to identify 3d conformation or organization of chains in space. The next section, section III, discusses the statistical quantities and our results by which we arrive at our conclusions. Section IV prescribes the method by which we can reconstruct in part the 3D conformation of the DNA polymer from the statistical quantities. We also hypothesize how this particular choice of CLs result in shaping the DNA-molecule. We end with summarizing our conclusions and discussions in the last section.

II. MODEL AND SIMULATION METHOD.

We use Monte Carlo simulations to explore the different microstates of the DNA chain. The DNA of bacteria *E. coli* is a ring polymer. We model *E. Coli* DNA with a bead spring model of ring polymer with $N_{EC} = 4642$ number of monomers in the ring. Thus, each model monomer bead represents 10^3 BPs. The DNA model-polymer is placed near the center of the simulation box of size $(200a)^3$ with periodic boundary conditions (PBC). The quantity a is the unit of length and is the average distance between two neighbouring monomer beads along the chain contour. The box size $L = 200a$ is chosen to be much larger than the expected maximum diameter of the polymer globule to keep the different diametrically opposite ends of the ring-polymer spatially apart from each even if PBC is invoked. The diameter σ of monomer bead is chosen to be $0.2a$. The Lennard Jones potential, suitably truncated at $r = 2^{1/6}\sigma$ and shifted (the Weeks Chandler Andersen-WCA potential) is used to model the excluded volume interaction between the monomers. Adjacent monomers along the chain are connected by a harmonic spring potential. $V(r) = \kappa(|\vec{r}| - a)^2$, where $|\vec{r}|$ is the distance between 2 monomers and a is the unit of length. We have chosen $\kappa = 200k_B T$, where the thermal energy $k_B T = 1$ is the unit of energy for our simulations.

Using data from [22] and subsequent analysis methods which are described in detail in the appendix, we obtained the frequency of finding two segments of *ecoli*-DNA spatially close to each other. We use this data from contact maps is used as input to our simulations. The experimental resolution of the size of segments is 10^3 base pairs. The model monomer in our simulations represents a DNA segment exactly of the same size as the experimental resolution. We cross-link monomers whose frequency of being found together be greater than threshold frequency p_c . The details of how this frequency map is obtained and analyzed is explained in Appendix-1. Depending on the value of threshold frequency that we choose, we can have (a) 47 (b) 159 pairs of monomers of the DNA-polymer which we cross-link. We number the cross-links (CLs) from 1 to N_{CL} , $N_{CL} = 49$ or $N_{CL} = 159$. We bind these pairs of monomers together by an additional spring potential $V_c = \kappa_c(r - a)^2$ with $\kappa_c = 20k_B T$. The cross-linked monomers are held together at a distance of a but the CLs can of course move with respect to each other as the chain explores different conformations.

The set of 47 CLs from biological contact-map data, which we refer to as BC-1 in the rest of the paper, are a subset of 159 CLs which we call BC-2. To analyze whether the overall meso-scale organization of the chain is determined primarily by a particular choice of CLs, we start our simulations from 9 very different and distinct initial conditions. For example, in one of the initial conditions the monomers of the ring polymer are arranged along a circle of radius $30.73a$ such that one circle has 193 monomers. The circle of monomers are stacked up

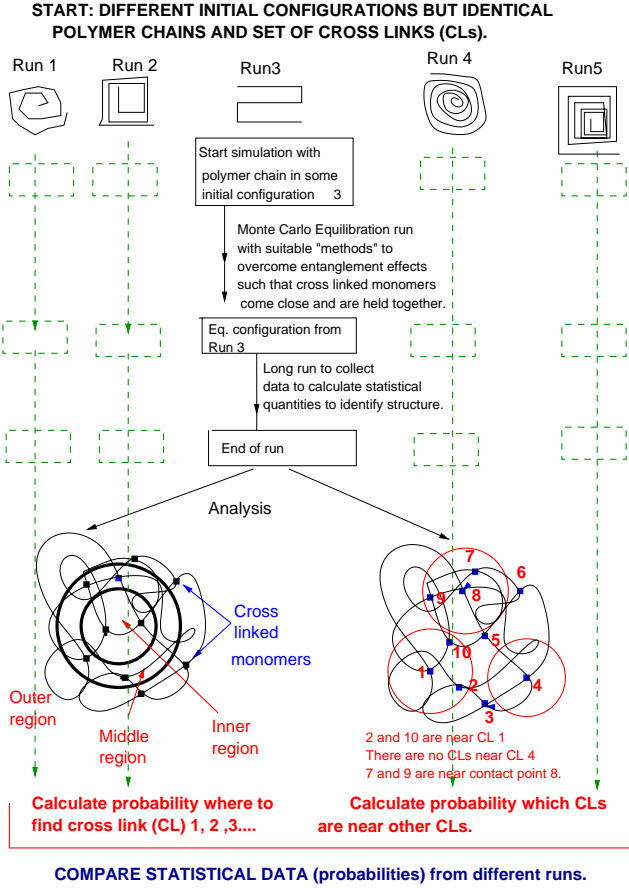


FIG. 1. Schematic diagram to give an overview of methodology used to ascertain if set of biologically determined constraint points (CL) lead to well defined organization of DNA-polymer chain. This statistical data is then contrasted with the case when the CLs constitute randomly chosen pairs of monomers along the polymer chain.

to form a cylinder. The first ring has monomer no. 1 to 193, the second ring has monomers 194 to 386 and so on. Note that this will lead to monomer numbered as 1 and the last monomer $N = 4642$ to be at a distance much larger than a though it is a ring polymer. In fact all the monomers which form CLs can be at distances much larger than a as they get arranged along the cylinder. But these will come closer as the polymer is allowed to relax during the MC run. In two other initial conditions we arrange the monomers in circles of radius $40.92a$ and $36.94a$. For the next three initial conditions, the monomers are arranged along squares of side $90a$, $80a$ and $70a$; these squares are stacked then up. For the last three initial conditions we arrange monomers in equilateral triangles of side $40a$, $50a$, $60a$ and stack them up to form a vertical column, by such initial conditions we have set up the CL monomers at rather arbitrary positions relative to each other in space without any consideration of CLs.

The question we then ask is: as the chain relax from their initial conditions to their equilibrium conformations

in different Monte Carlo runs, do all of them organize themselves (averaged over thermal fluctuations) in some particular set of conformations which is determined by the set of CLs? After relaxation to the equilibrium state, if we compare equilibrium conformations from different runs, are the organization of monomers the same (in a statistical sense) though the chain has started out from very different initial conditions? This idea is schematically represented in Fig. 1.

We clarify here that we use certain tricks to allow the chain to relax slowly over 10^5 Monte Carlo iterations to its equilibrium state without allowing the system to get stuck in some entangled and metastable state. We set spring constant of cross-links $\kappa_c^{initial} = 0.01\kappa_c$ at the start of the simulation and gradually ramp it in steps of $0.01\kappa_c$ every 1000 MC steps, as the CL monomers approach each other in the relaxation process. In a standard Metropolis step, a monomer attempts a displacement $\vec{dr} = \delta(r_1\hat{i} + r_2\hat{j} + r_3\hat{k})$ in a random direction, where $\delta = 0.2a$ and r_1, r_2, r_3 are random numbers. The attempt is accepted with Boltzmann probability. In addition, every 100 iterations, we attempt displacements with $\delta = 1.2\sigma$. This helps chains to cross each other sometimes and overcome topological constraints which might arise as the chain relaxes from its initial condition.

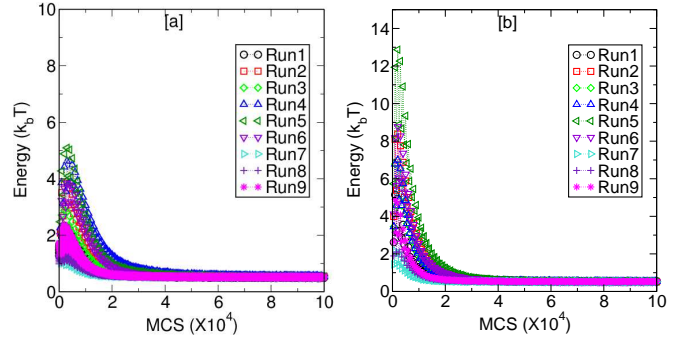


FIG. 2. Plot of the energy versus Monte Carlo steps (MCS) as the systems evolve to a relaxed state from the 9 different initial conditions. The energies all converge and fluctuate around the same value establishing that the chains are *probably* not stuck in some metastable states due to topological constraints arising from excluded volume interactions. Subplot (a) and (b) are for 47 and 159 CLs respectively. Statistical quantities to determine structure start after the system relaxes to equilibrium.

We monitor the potential energy as the chain relaxes and see that the value of energy relaxes to the same value at the end of 10^5 iterations from the 9 different runs, refer Figure 2. This gives us confidence that the chain conformations are not stuck at metastable energy minimum due to entanglements. From this relaxed state reached after 10^5 MC iterations, we evolve each of the 9 different chain conformations in independent simulation runs over the next 12×10^6 iterations and collect data to calculate structural quantities and compare the results. We carry out this comparison of statistical data from 9 indepen-

dent runs for each set of CLs, viz., chains with (a) 47 (b) 159 CLs.

In addition, we also carry out similar calculations starting from 9 independent configurations for 2 sets of randomly chosen position of CLs, i.e. the monomers which are cross-linked together are chosen randomly from the list of monomers. In BC-1 and BC-2 set of CLs, there are some CLs which are not independent. For example monomer numbered 16 and 17 are cross linked to monomer 2515 and 2516, respectively. One cannot consider them as distinct CLs. The list of cross linked monomers is given in Table-1 of Supplementary section I. Hence there are fewer effective CLs than the number of CLs in BC-1 and BC-2. Thus we compare the results of our simulation from bio-CLs (BC-1 and BC-2) with equal number of *effective* random CLs. In each of these random set of CLs, we have exactly the same number of *effective* CLs as the ones obtained from biological data, which is actually less than the corresponding number of CLs in BC-1 and BC-2. Hence the list of randomly positioned CLs have just (a) 27 effective number of CLs (we refer these as RC-1) and (b) 82 effective CLs (referred as RC-2), corresponding to 47 CLs in BC-1 and 159 CLs in BC-2. We can now compare structural data obtained from polymer simulations using BC-1 and RC-1 on one hand, and BC-2 and RC-2 on the other.

III. RESULTS

Now we discuss the statistical quantities which we use to investigate the structure and conformation of the DNA polymer. We collected data every 5 MC steps over $N_{it} = 12 \times 10^6$ iterations to calculate average of various statistical quantities after the chains relax to local equilibrium states in 2×10^5 iterations from 9 different initial configurations. We check if statistical quantities from 9 different runs with the same set of CLs give similar results in order to infer that the polymer has similar shape and conformation across runs.

The first quantity we want is an estimate of the size and extent of the DNA-polymer globule with CLs. To that end, we calculate the moment of inertia tensor \mathbf{I} with respect to the center of mass (CM) of the polymer globule and diagonalize the matrix to get its principal moments for each microstate. We then calculate the average of the principal moments I_1, I_2, I_3 .

In Fig 3(a) and (c) we show the values of I_1/I_3 and (b) $R_g = \sqrt{(I_1 + I_2 + I_3)/3M}$ for sets of bio CLs and random CLs. Here M is the sum of masses of the individual monomers $M = \sum m_i$, $m_i = 1$ is the mass of each monomer. The value of I_1/I_3 is the ratio of major and minor axes, and gives a measure of shape asymmetry of the globule. The fluctuations in I_1/I_3 are of similar scale for BC-1 and RC-1, the fluctuations are lower for RC-2 compared to that for BC-2 data, moreover the value of I_1/I_3 is lower for RC-2 compared to BC-2. A plausible explanation for this difference is given later in this para-

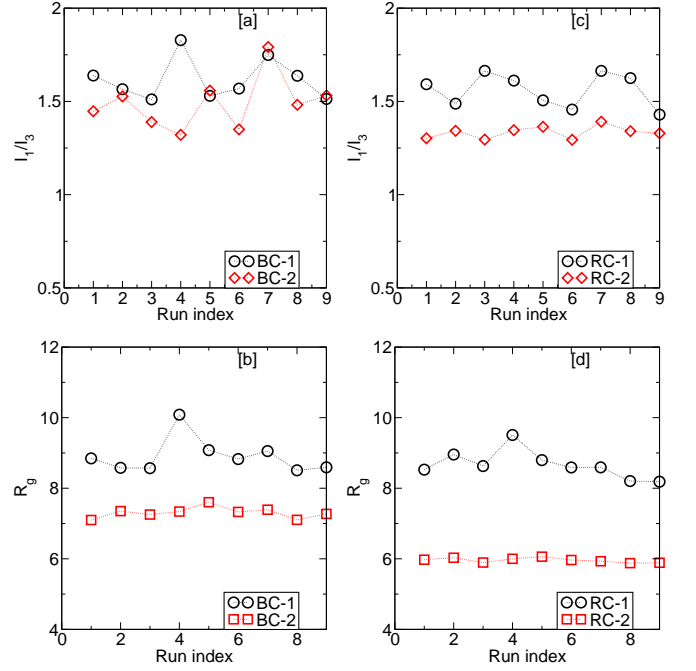


FIG. 3. (a) The value of I_1/I_3 , the ratio of the largest and lowest eigenvalues of the diagonalized moment of inertia matrix versus run-index from 9 independent initial conditions for biologically determined CLs: BC-1 and BC-2. (b) Plot of Radius of gyration $R_g = \sqrt{(I_1 + I_2 + I_3)/3M}$ on y-axis versus run index on the x-axis. (c) I_1/I_3 versus run-index for CLs chosen randomly: RC-1 and RC-2. Subplot (d) shows R_g versus run-index for random CLs: RC-1 and RC-2.

graph and at the end of this paper. Subplots Fig 3 (b) and (d) show the values of R_g obtained from 9 independent runs with BC-1, BC-2, RC-1 and RC-2 CLs. The value of R_g decreases as we increase the number of CLs from BC-1/RC-1 set to BC-2/RC-2 set; this decrease in the value with increase in the number of *effective* constraints is expected. But interestingly, the change in the value of R_g as we go from BC-1 to BC-2 is distinctly less than the decrease in R_g as we go from RC-1 to RC-2. We interpret the difference between the two cases as follows: the *effective* CLs in BC-1 are already at critical positions along the contour which give partial organization in the DNA. On increasing the number of CLs (BC-2), the organization of the molecule improves along the already established framework. On the other hand, increase in the number of random CLs leads to an overall shrinkage in the size of globule and not necessarily to accentuate a preferred set of conformations. The lower values of I_1/I_3 for RC-2 compared to that in BC-2 also point towards such an understanding. This idea will get further substantiated in the rest of the paper.

To get an idea of how the monomers of the polymer are distributed in space and if there is any difference in the radial arrangement of bio-CLs and random CLs, we investigate the radial distribution of monomer number densities and the normalized CL number density with the

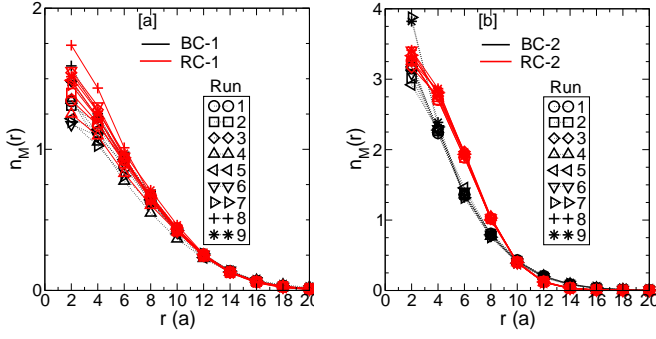


FIG. 4. The monomer number density of $n_M(r)$ is plotted versus r , where r is the distance of the position of the monomers from the center of mass of the DNA-polymer coil. Plot [a] is for BC-1 and RC-1, whereas subplots (b) are for BC-2 and RC-2.

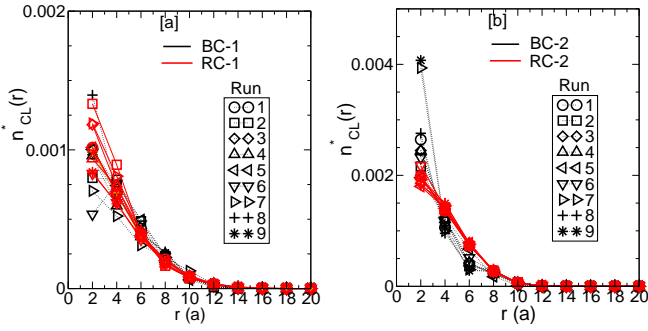


FIG. 5. The normalized CL number density of $n_{CL}^*(r)$ is plotted versus r , where r is the distance of the position of the CLs from the center of mass of the DNA-polymer coil. Subplot [a] is for BC-1 and RC-1, whereas subplot (b) are for BC-2 and RC-2. The number of CLs in each case is further normalized by the total number of CLs in each case.

distance r from the center of mass (CM) of the polymer coil. The quantities $n_M(r)$ and $n_{CL}(r)$ are calculated by calculating the average number of monomers and CLs in radial shells of width $2a$ from the CM of the coil, divided by the volume of each shell. The CL-density is further normalized by the total number of CLs for the particular case under consideration to obtain $n_{CL}^*(r)$. Data for $n_M(r)$ and $n_{CL}^*(r)$ from 9 independent runs are plotted for each of set of CLs: BC-1, BC-2, RC-1, RC-2 in Figs.4 and 5, respectively. The data in each of the subplots from 9 independent runs lie on top of each other, an indication that the arrangement of monomers and CLs have relaxed to similar distributions and is independent of starting configuration of monomers.

Comparing subplots (a) and (b) of Figs. 4 and 5 for BC-1 and BC-2, establishes that coils with higher number of CLs lead to more number density of monomers and CLs at the center. As the coil gets into a more compact globule structure with RC-2, we again see an increase in the number density of monomers, CLs (suitably normalized) compared to the values obtained for RC-1. Comparing data for BC-1 and RC-1 (subplots (a) & (c) and

(b) & (d)), respectively from Figs. 4 and 5, we observe that $n_M(r)$ of monomers and CLs are similar in values at different r . It implies that the positions of CLs in BC-1 and RC-1 do not bring in any difference in the radial distribution of monomers and CLs. In contrast, the normalized density of CLs at the central region is more for BC-2 compared to that for RC-2 though monomer density does not show any significant difference. Lastly, the number density of monomers/CLs drops down significantly beyond a distance of $8a$ from the coil's center.

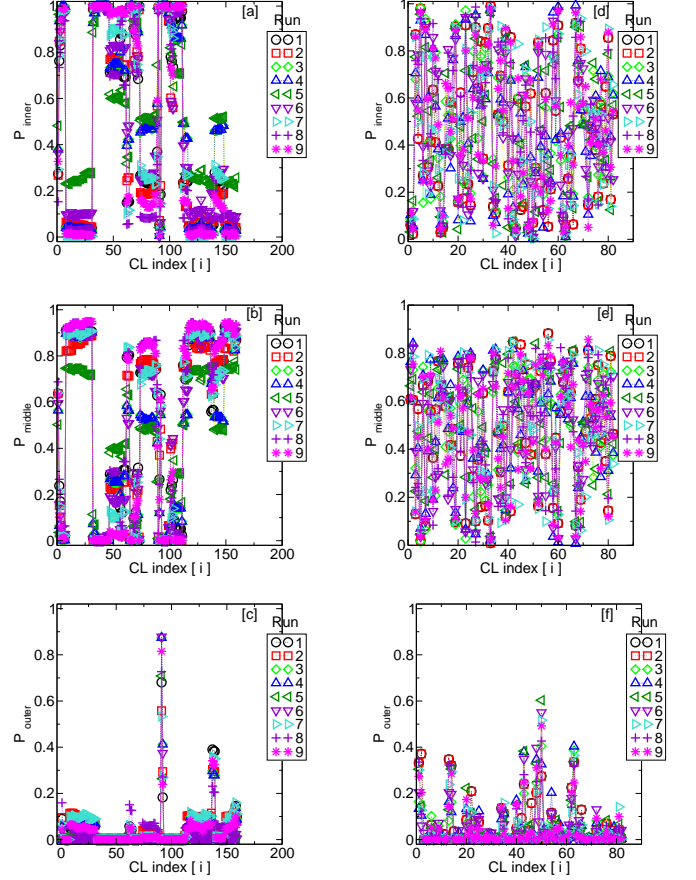


FIG. 6. Subplots [a], [b] and [c] (on left column) shows the probabilities of individual CLs to be found in the inner, middle and outer region for CL-set BC-2. The x-axis is CL index. Data for runs from independent runs starting from different initial conditions are shown by different symbols. Data from different runs indicate that the probability of finding CL i is the same from different runs. Data [d], [e], [f] on right column is for set of random CLs RC-2. The set of 159 CLs for ecoli are referred to as BC-2. Data set with fewer number of ecoli and random CLs (referred as BC-1 and RC-1, respectively) are shown in Supplementary Section Fig.19.

To gain some more idea about the global structural organization of the DNA-globule, the simplest question to ask is whether a particular CL is always found near the center of the coil or near the periphery of the coil. To this end, we compute the probability of each of the CLs to be found in the *inner*, *middle*, and *outer*

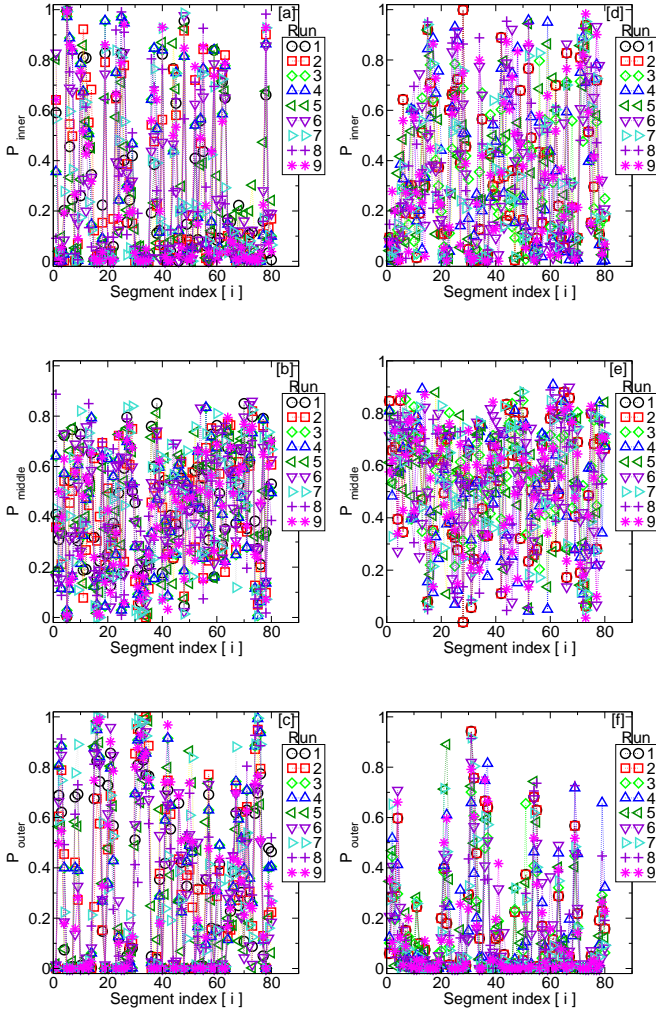


FIG. 7. Subplots [a], [b] and [c] (on the left column) shows the probabilities of the center of mass (CM) of 80 dna-polymer segments to be found in the inner, middle and outer region of *ecoli* DNA globule. The x-axis is segment index. The different lines are from independent runs starting from different initial conditions. Data from different runs indicate that the probability of finding CM of segment i in a particular region is nearly the same across different runs. Data on subplots [d], [e], [f] is for random choice of cross-link position (set RC-2) with 82 CLs in a chain with 4642 monomers. Each segment has 58 monomers, the dna-polymer has around 80 segments. Data set with fewer CLs (referred as BC-1 and RC-1, respectively) are shown in Supplementary Section Fig.20.

regions of the DNA-globule. We use the cutoff radii $R_{inner} = 5a$, $R_{middle} = 9a$ (chosen from the knowledge of the value of $R_g \approx 8a$) and calculate the probability $P_{inner}, P_{middle}, P_{outer}$ of finding the p -th CL at a distance $r < R_{inner}$ (inner region), $R_{inner} < r < R_{middle}$ (middle region) and $r > R_{middle}$ (outer region), respectively. If the values of $P_{inner}, P_{middle}, P_{outer}$ for each CL is similar in value in each of the 9 independent runs, it would indicate that the presence of CLs lead to similar

organization of the DNA across runs. Also we compare the probability distribution of CLs for runs with bio-CLs and random-CLs to investigate if bio-CLs lead to organization distinct from that obtained with random-CLs.

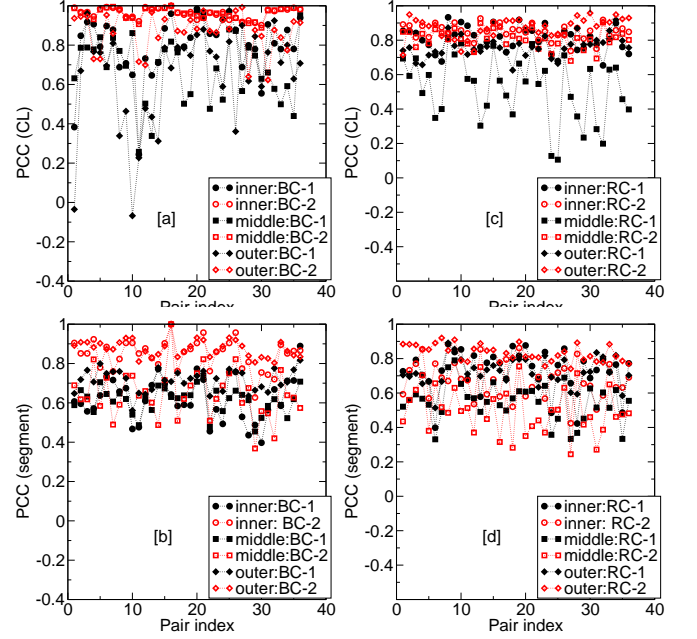


FIG. 8. Pearson correlation coefficient (PCC) for $P_{inner}, P_{middle}, P_{outer}$ data obtained from pairs of different runs (data from Figs.6 and Figs.7) to show that the radial distribution of CL/segment locations are correlated across different runs. There are 9 independent runs, and ${}^9C_2 = 36$ combinations of pairs can be used to calculate PCC. The x-axis refers to the index of 36 pairs of runs chosen to calculate PCC. PCC for radial distribution of CLs using BC-1, RC-1 are shown in subplot (a), subplot (b) shows PCC for BC-2 and RC-2. PCC for radial distribution of segments using BC-1, RC-1 are shown in subplot (c), PCC for segments using BC-2 and RC-2 are in subplot (d).

We carry out the same exercise for different segments of the polymer chain. The *E. Coli* chain with 4642 monomers is divided into 80 segments with 58 monomers in each of segment and the segments are labelled from $i = 1, 2, \dots, N_s$ as we move along the contour. We can then calculate the location of the CMs of each segment, and find out the probability of finding the CMs in the central, middle and outer region. The segments in a random-walk polymer model without CLs can take any conformation, and there is no reason to believe that certain segments will preferably be found in the inner or outer regions of the coil. If the segments were completely delocalized, we would expect the polymer in different microstates to contribute to all the $P_{inner}, P_{middle}, P_{outer}$ quantities for each segment. The question is to what extent will this basic behaviour of polymer coils get modified by the presence of bio-CLs and random-CLs?

Probability data about the location of CLs and segments for BC-2 and RC-2 is given in 6 and 7, respec-

tively. Data for BC-1 and RC-1 is given in the Supplementary data section Fig.20. From each run the value of $P_{inner} + P_{middle} + P_{outer}$ must remain = 1 for each CL and each segment. Furthermore, from Figs 6 and 7(a),(b) and (c) we see that the probability of a particular CL/segment to be high in (say) inner region remains high across all 9 runs. Correspondingly, the values of P_{middle} and P_{outer} remain low in all the runs. But there are statistical fluctuations in the value of probabilities across different runs. Some CLs, e.g. the CL with index 60 has nearly equal probability to be in the inner or middle region of the coil, but very low probability to be found at the outer region.

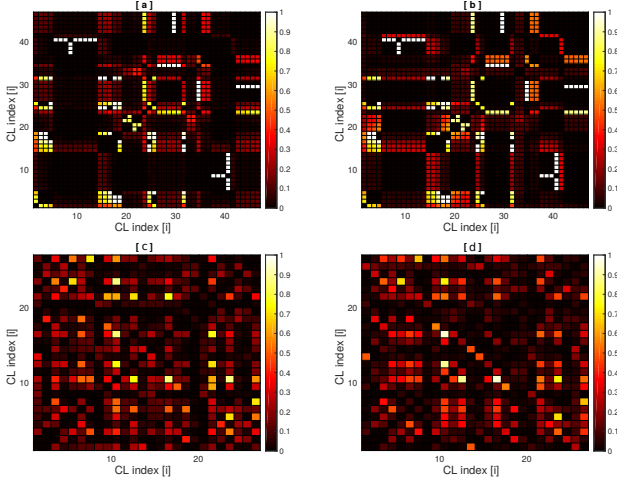


FIG. 9. Colormaps to represent probability to find CLs i spatially close CLs j . The top 2 figures are for runs with BC-1 with 47 CLs ($i, j = 1..47$) and the bottom two subplots are with RC-1 with $i, j = 1, \dots, 27$. More colormaps from independent runs are given in Supplem. Section: Fig.21

To ensure that we get equivalent probability data sets of CLs in the inner, middle and outer regions of the coil, we calculate the Pearson Correlation Coefficient (PCC) to compare the values of $P_{inner}, P_{middle}, P_{outer}$ of the same CLs/segments from different runs. We can pair up probability data from 9 independent runs in ${}^9C_2 = 36$ pairs of probability data for each of P_{inner}, P_{middle} and P_{outer} quantities. The expression PCC is given by

$$PCC = \frac{\sum_1^{36} (x_i - \bar{x})(y_i - \bar{y})}{\sqrt{(\sum x_i - \bar{x})^2} \sqrt{(\sum y_i - \bar{y})^2}} \quad (1)$$

Here, x_i is the value of probability (P_{inner} or P_{middle} or P_{outer}) for CL index for a particular run, y_i is the value of P for the same CL index i from another run, \bar{x} and \bar{y} is the average of x_i and y_i from their respective runs. The value of PCC for a pair of runs gives whether the data from the two runs are correlated or not. That means if CL index i has a high value of $P_{middle}(i)$, and CL- $i + 1$ has low value of $P_{middle}(i + 1)$ (and so on for each CL index) in Run-1, does the $P_{middle}(j)$ values of CL indices $j = 1, 2, \dots, N_{CL}$ from Run-2 show similar

trends? If PCC values are close to 1 for a pair of runs for inner/middle/outer region, we can conclude that structural organization obtained from the 2 different runs are similar. If PCC values are ≈ 0 , then we set probability data sets from 2 different runs are uncorrelated. The data for PCC calculated for CL indices as well as segment indices for bio and random data are shown in Fig.8. The value of PCC is shown in Fig 8 for CL-positions and segment CMs: we consistently get high correlation values for inner/middle/outer regions. This indicates that the radial distribution of CLs and segments in the inner/middle/outer regions are much the same across different runs.

Having established that the CLs and segments of DNA-polymer globule have some degree of radial organization, we try to extract more detailed structural information about the position of segments relative to each other within the globule. We calculate the probability of each CL (of each segment) to be in close proximity to other CLs (other segments). If there is no particular well defined relative position of CLs/segments within the chain-globule, there is no reason to expect CM of certain segments (or independent CLs) to be found spatially close to each other with high probability, especially when the segments/CLs are separated along the chain contour. We define two CLs/segment's CM to be close to each other if the distance r between the CLs/segment-CMs are $< 5a$, which is just more than $0.5R_g$. We emphasize that we have cross-linked monomers, these constraints are at the monomer (1000 BP) length scale, whereas we are investigating the organization of polymer segments at a much larger length-scale. The position of CLs and position of CM of segments are just 2 different markers of different sections of the chain, and we use relative position of both to identify spatial correlations between different sections of the chain.

In Figs. 9, 10 we show colormaps showing the average probability $p(i, j)$ of finding each pair CLs i, j at distances of $< 5a$ for BC-1, RC-1 and BC-2, RC-2 respectively. As the Monte carlo simulation evolves, at each different microstate if the distance d between every pair of CLs is such that $d < 5a$, a counter $c(i, j)$ for pair i, j is incremented. The probability $p(i, j)$ at the end of the MC-run is the value of $p(i, j) = c(i, j)/N_{micro}$, where N_{micro} is the number of microstates over which data is calculated for calculation. The x-axis and the y-axis represent CL indices i, j , and the colored pixel indicates the probability of two CLs to be close to each other: lighter color (white) indicates $p(i, j)$ values close to 1, darker colors indicate lower probabilities. The top two colormaps of Figs.9 (and Fig.10) represent data obtained BC-1 (and BC-2) from two runs starting from different initial conditions, the bottom two colormaps of Figs.9 (and Fig.10) show data from two runs for RC-1 (and RC-2) set of CLs.

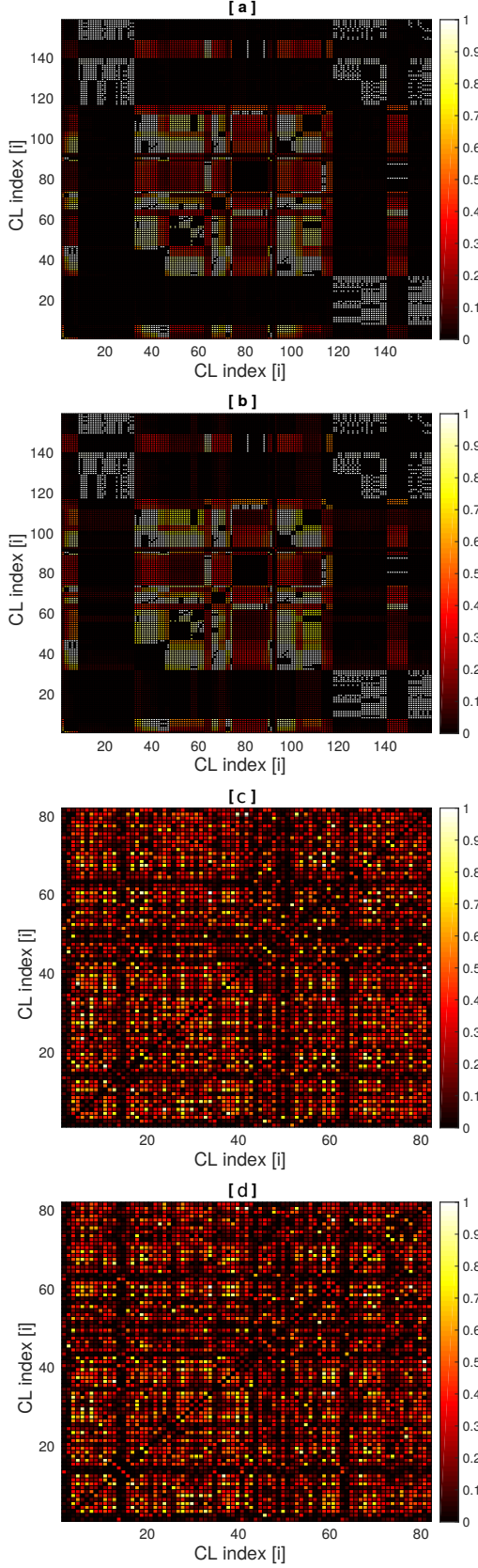


FIG. 10. Colormaps to represent probability to find CLs i spatially close CLs j . The top 2 figures are runs with BC-2 with 159 CLs ($i, j = 1 \dots 159$) and the bottom two subplots are with RC-2 with $i, j = 1, \dots, 82$. More colormaps from independent runs are given in Supplem. Section: Fig.23

A pair of CLs which are near each other along the contour of the chain will have the distance $d < 5a$ between them by default, and will show up as high probabilities in the colormap. We set these $p(i, j) = 0$ in the calculation, if the monomers constituting pair of nearby CLs are separated by less than 6 monomers along the contour. We do this because we want to see only non-trivial correlations between different CLs. Following Figs. 9, 10, the colormaps show probability of finding a pair of segment-CMs within distance of $5a$ for BC-1/RC-1 and BC-2/RC-2 is shown in Figs.11 and 12, respectively. Note that these probability colormaps give much more detailed information than a pair correlation function $g(r)$, which would just give the average distance between CLs or segment-CMs.

We arrive at a number of conclusions by comparing different pairs of probability-colormaps in Figs. 9,10,11 and 12. Firstly, comparing colormaps for data from different initial conditions, e.g. compare the top two colormaps in each of the figures which are for BC-1/BC-2 (or equivalently compare the bottom two colormaps which are for RC-1/RC-2), shows bright and dark patches at equivalent positions in the map. Thus the same set of CLs and segments are spatially near each other in both the runs, i.e. the polymer organization is similar in both the runs. Additional colormaps from two more independent runs for each set of CLs are also given in the Supplementary section for further comparison. The reference to relevant colormaps in Supplementary section is given in the figure caption of each figure, and these further reiterates our conclusion that the structural organization of DNA-polymer is similar across different runs for the same set of CLs. Thus we find further evidence of our hypothesis that the set of CLs decides the large scale structure of the polymer.

Secondly, the number of the bright pixels are much more in colormaps obtained using CL sets BC-2 and RC-2 (Figs. 10 and 12) as compared to colormaps for BC-1, RC-1 (Figs. 9 and 11, respectively). This is not surprising as more CLs lead to relatively more compact well defined structure, and a large number of CLs (or segments) near one another. With the few bright patches for BC-1, RC-1 CL set with 27 *effective* CLs, one cannot clearly define the meso-scale conformation of the whole chain, though there are indications of emergence of structure. However, a set of 82 effective CLs for BC-2, RC-2 might be enough to deduce and define the large scale organization of DNA-polymer as we now know which segments are neighbours of any particular segment.

Thirdly, comparison of colormaps for BC-2 and RC-2, especially in Figs. 12 show a different nature of organization of the DNA polymer. For BC-2 adjacent segments show higher propensity to be together, which can be deduced by observing that there are clusters of adjacent bright pixels. Comparatively, bright pixels are scattered more randomly in the colormaps for RC-2. The BC-2 colormap is reminiscent of the fractal globule structure of DNA suggested by other researchers [7, 25, 26].

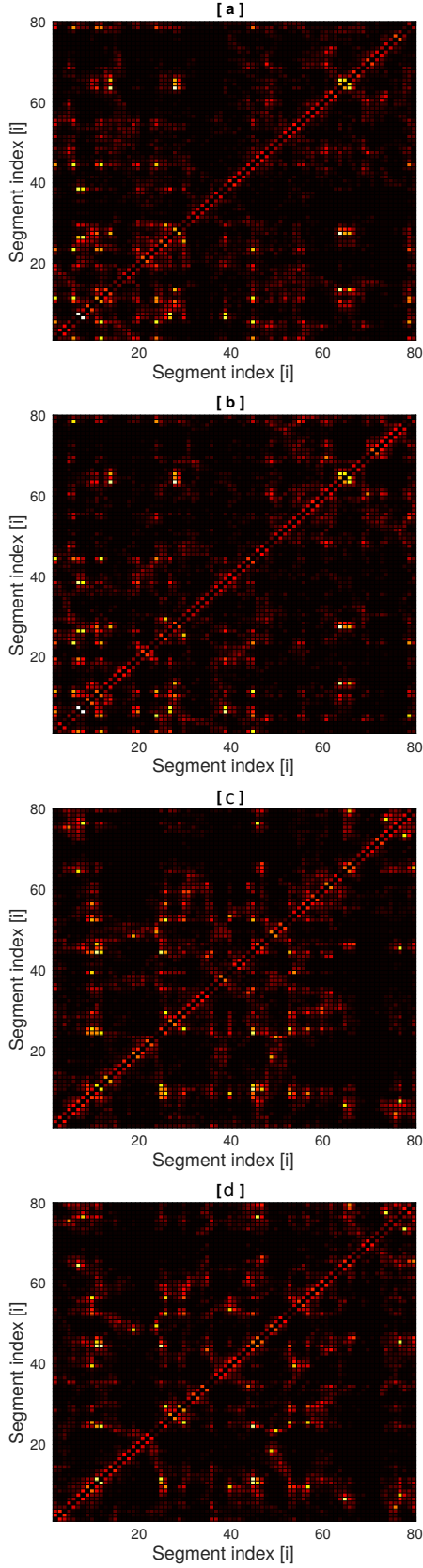


FIG. 11. Colormaps to represent probability to find CM of segment i spatially close to CMs of other chain segments j . There are 80 segments in the *E. Coli* polymer with 58 monomers per segment. The top 2 figures are runs with BC-1 and the bottom two for RC-1. More colormaps from independent runs are given in Supplem. Section: Fig.22

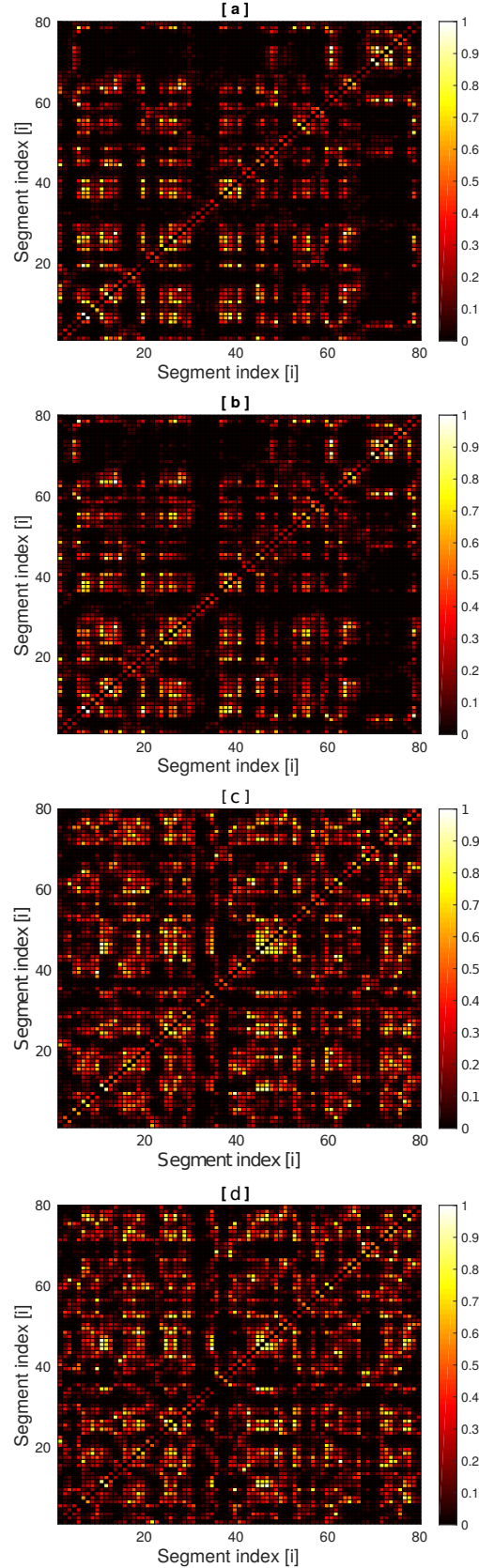


FIG. 12. Colormaps to represent probability to find CM of segment i spatially close to CMs of other chain segments j . There are 80 segments in the *E. Coli* polymer with 58 monomers per segment. The top 2 figures are runs with BC-2 and the bottom two subplots RC-2. More colormaps from independent runs are given in Supplem. Section: Fig.24

In fractal globule structure, adjacent segments along the contour length of the chain are found close to each other with higher probabilities compared to probabilities of finding together two remote segments of the chain. The organization of segments as seen from the colormap of Fig.12 seem to match with this understanding. We do not calculate scaling exponents to establish that the fractal globule structure of the chain as our globule is too small ($R_g \sim 6a$) to be able calculate relevant exponents. Observing the differences in colormaps for BC-2 and RC-2, we claim that the position of CLs along the chain for DNA are not completely random. An equivalent number of CLs in random positions also give an organized structure, but the nature of organization is very different from the biological position of CLs.

Fourthly and importantly, the reasons for the formation of clusters of bright pixels seen in the top two colormaps of Figs. 9 & 10 (for CLs) is not the same as of Fig.12 (for segment-CMs). To understand the bright patches of Figs 9 & 10, we remind the reader that the CLs are often found adjacent to each other along the chain contour for BC-1 and BC-2. Suppose, CL- i , CL- j and CL- k are next to each other along the chain. Note that then $p(i, j)$, $p(i, k)$, $p(j, k)$ has been explicitly put to zero. But if CL- m , which is far from i and j along the contour, comes within a distance of $5a$ from CL- i , then CL- m is also automatically close to CL- j , k and three adjacent pixels will appear in the colormap, viz., $p(i, m)$, $p(j, m)$, $p(k, m)$. Thus, the bigger bright patches for BC-2 in Fig. 10 should not necessarily be interpreted as evidence for a more organized polymer. Similar arrangement of bright/dark pixels across runs is just evidence of similar organization across different runs. We do not get big bright patches in the colormaps for RC-1 and RC-2 in Figs. 9 & 10, because the calculation are done using only the *effective* number of CLs. Thereby there are no redundant CLs in the RC-1, RC-2 set of CLs.

To extract further insight into the structural organization of the DNA-polymer, we would next probe whether the allowed conformations of the polymers are severely restricted by the presence of CLs. If so, can we decipher whether some segments are at geometrically fixed positions with respect to each other, of course accounting for thermal fluctuations. We calculate next the angular correlations between CLs and equivalently between segment's CMs.

To that end, we calculate the dot product of the radial vectors from the CM of the polymer-globule to the respective positions of a pair of CLs (i, j) and check if the value of $\cos(\theta_{ij}) > 0$ or < 0 , where θ_{ij} is the angle between the two vectors. If the value of $\cos(\theta_{ij}) > 0$, we can say that the two CLs are on the same side/hemisphere of the globule, and increment counter $c^{opp}(i, j)$ by 1. If $\cos(\theta_{ij}) < 0$ we decrement $c^{opp}(i, j)$ by 1. For all possible pairs of CLs, we calculate the average value of $\langle c^{opp}(i, j) \rangle$ suitably normalized by number of snapshots used to calculate the average. The value of $\langle c^{opp}(i, j) \rangle \approx -1$ would indicate that the pair of CLs i, j are always on two op-

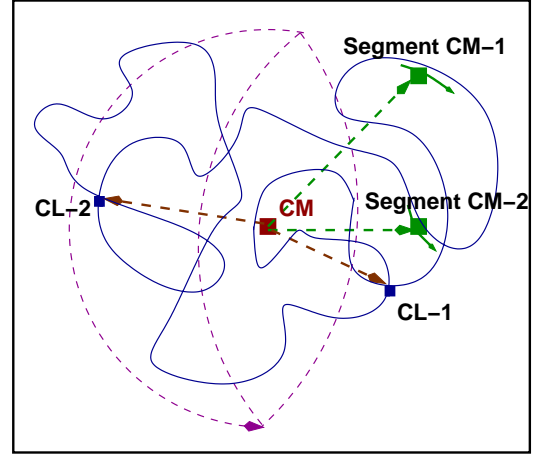


FIG. 13. A schematic diagram showing a representative polymer coil in continuous blue line. The angle between vectors joining the center of mass (CM) of the coil to the cross-links CL-1 and CL-2 is more than 90, such that $\cos(\theta) < 0$ and the CLs lie on opposite hemispheres (showed in dashed line). On the other hand the center of mass of two segments of the polymer, labelled as segment CM-1 and segment CM-2, are within the same hemisphere. This schematic diagram explains the calculation of $\langle c^{opp}(i, j) \rangle$ (see text) which in turn is used to provide information the relative angular positions of different CLs and segments of the DNA-polymer.

posite hemispheres. A value of $\langle c^{opp}(i, j) \rangle \approx 1$ means that the two CLs remain on the same hemisphere. The motivation for this calculation is further explained in the schematic diagram in Fig.13. We should not interpret $\langle c^{opp}(i, j) \rangle \approx 0$ as we cannot claim that the average angle between the radial vectors is nearly a right angle. The reason is that if the CLs are closer to the center of the DNA-globule, small positional displacements could cause the quantity $c^{opp}(i, j)$ to fluctuate between 1 and -1 and cause $\langle c^{opp}(i, j) \rangle$ to average out to zero. The $\langle c^{opp}(i, j) \rangle$ data for all pairs of CLs are given in Figs.14 & 15 for BC-1/RC-1 and BC-2/RC-2 respectively, the corresponding data for relative angular positions for segment CMs are given in Figs.16 & 17 for BC-1/RC-1 and BC-2/RC-2. As before, the top two colormaps in all the four figures are from two independent initial conditions with BC-1/BC-2 and the bottom two colormaps are for two independent runs with RC-1/RC-2.

In the colormaps of Figs.14,15,16 and 17 we see there are large patches of bright and dark pixels. Bright pixel corresponds to the value of $\langle c^{opp}(i, j) \rangle = 1$: two CL/segment's CM are in the same hemisphere across the simulation run. A dark pixel corresponds $\langle c^{opp}(i, j) \rangle = -1$ i.e. two CLs/segment's CM lie on two opposite hemisphere. And if $\langle c^{opp}(i, j) \rangle = 0$ which is represented by orange color in the colormap we cannot predict the angular positions of the CLs/segment's CMs because of the reason explained above. We can clearly see that the colormaps from different initial conditions look similar.

In figure 16, comparing segment-CM colormaps in

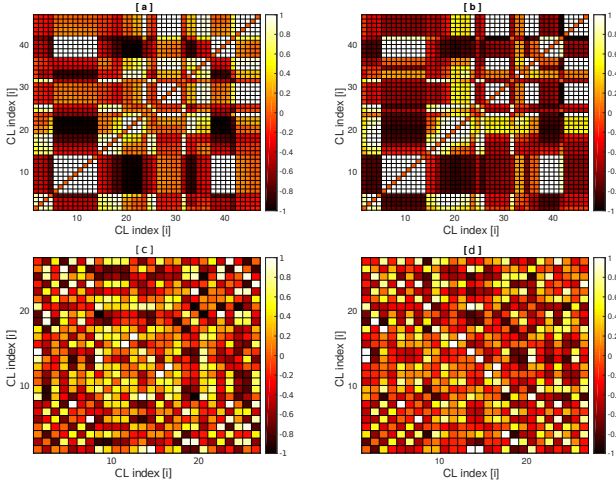


FIG. 14. Colormaps to investigate the angular location of different CLs respect to each other. Subplots (a),(b) are for BC-1 and (c),(d) for RC-1 with different initial conditions, respectively. The data shows the probability of two CLs to be on the same or opposite side of the globule. Refer the text for more details and Supplementary section Fig.25 to compare more colormaps from independent runs.

(a),(b) (for BC-1) with (c),(d) (for RC-1) we do not find any difference in the nature of distribution of patches. But as the number of CLs become more as we go from BC-1 to BC-2 and RC-1 to RC-2 in Fig.17, we find differences in the pattern of colormaps on comparing (a),(b) with (c),(d) corresponding to BC-2 and RC-2 CL sets, respectively. In colormaps (a),(b) of Fig.17 we observe large patches of bright pixels as compared to the patches in (c),(d). Large patches of bright/dark pixels suggest adjacent segments are on the same/opposite hemispheres with respect to the CM of the globule. This interpretation is similar to that of the colormaps of Fig.12 and strengthens our interpretation of fractal globule organization of the DNA-polymer for bio-CLs. The small patches of bright and dark pixels in (c),(d) for RC-2 suggest more of random distribution of different segments which is similar to equilibrium globule suggested in literature [26]. The polymer is organized in both BC-2 and RC-2 CL sets, but the nature of the organization is different.

The reasons for large bright patches in the colormaps for CL-angular positions as shown in Fig.14,15 is not same as for the colormaps in Fig.17. The reasons for the difference has been explained previously for positional correlation colormaps.

Finally, we show a representative snapshot of the DNA-polymer Fig.18 (top) is a snapshot from a simulation. The polymer is colored from blue to red along the contour. This snapshot confirms what we have deduced from the previous figures of positional and angular correlations. Large sections of the chain are localized together in space as one would expect for a fractal globule structure.

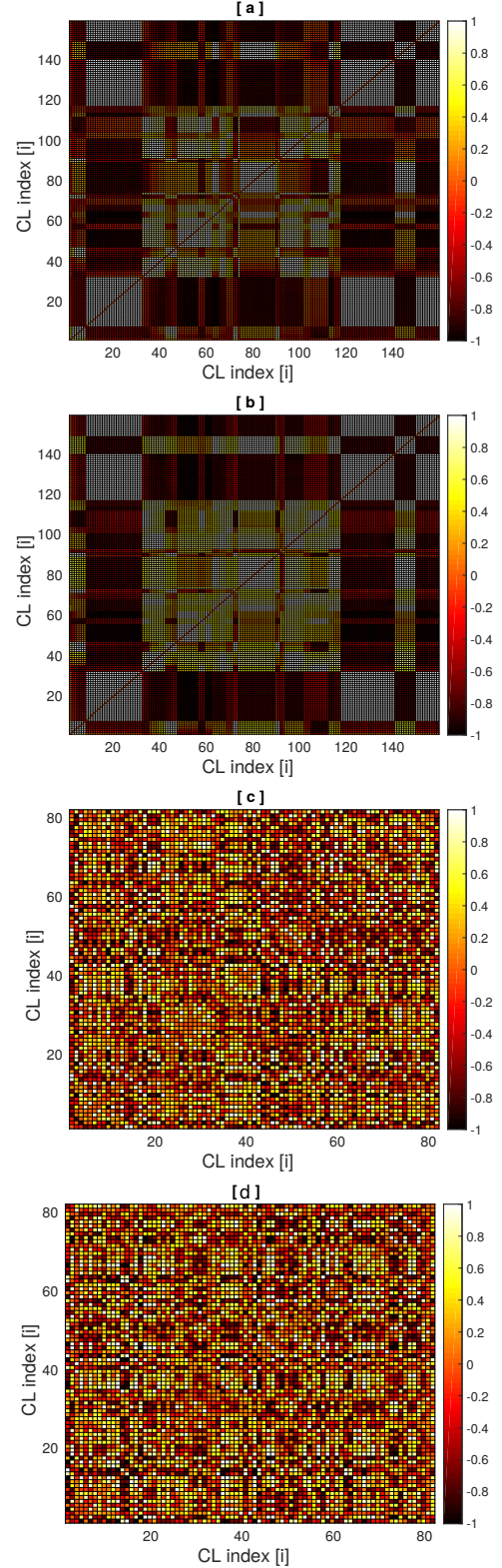


FIG. 15. Colormaps to investigate the angular location of different CLs with respect to each other. Subplots (a),(b) are for BC-1 and (c),(d) for RC-1 with different initial conditions, respectively. Refer Supplem. section Fig.26 to compare with more colormaps from independent runs.

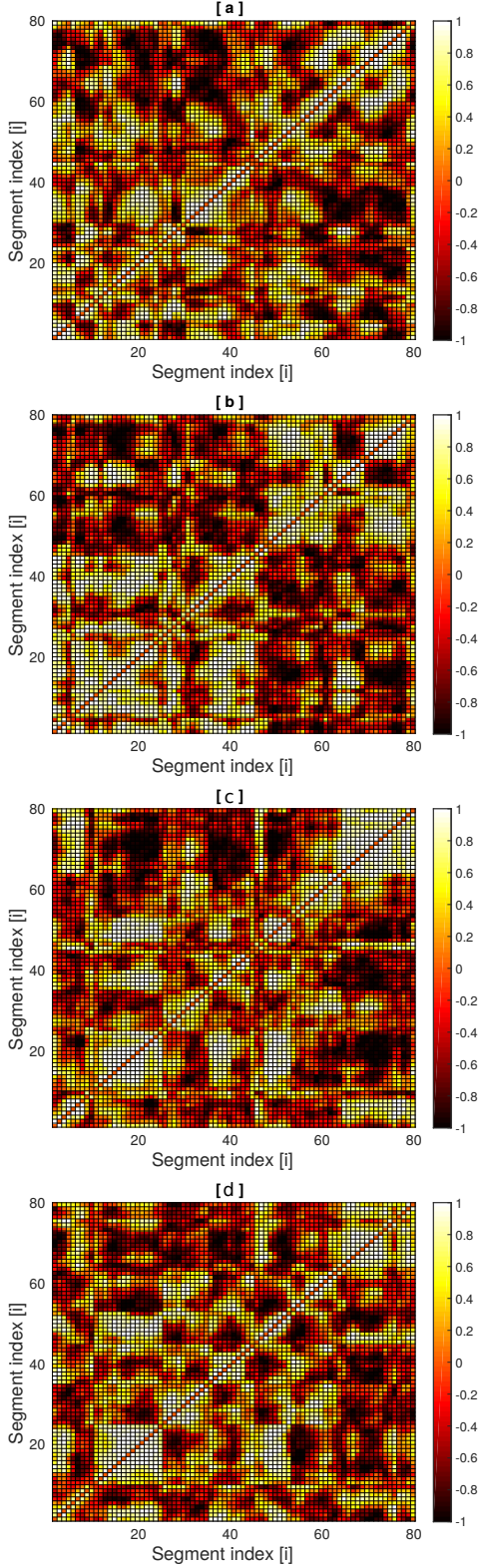


FIG. 16. Colormaps to investigate the angular location of different dna-polymer segments respect to each other. Subplots (a),(b) are for BC-1 and (c),(d) for RC-1 with different initial conditions, respectively. Refer Supplem. section Fig.27 to compare with more colormaps from independent runs.

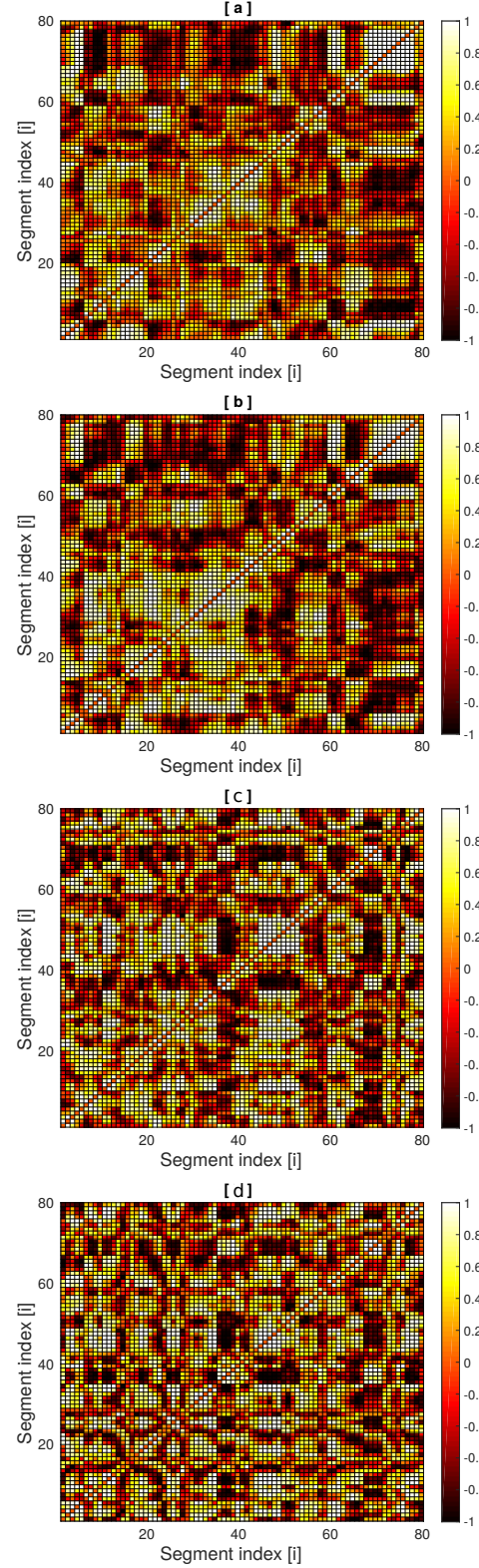


FIG. 17. Colormaps to investigate the angular location of different dna-polymer segments respect to each other. Subplots (a),(b) are for BC-2 and (c),(d) for RC-2 with different initial conditions, respectively. Refer Supplem. section Fig.28 to compare with more colormaps from independent runs.

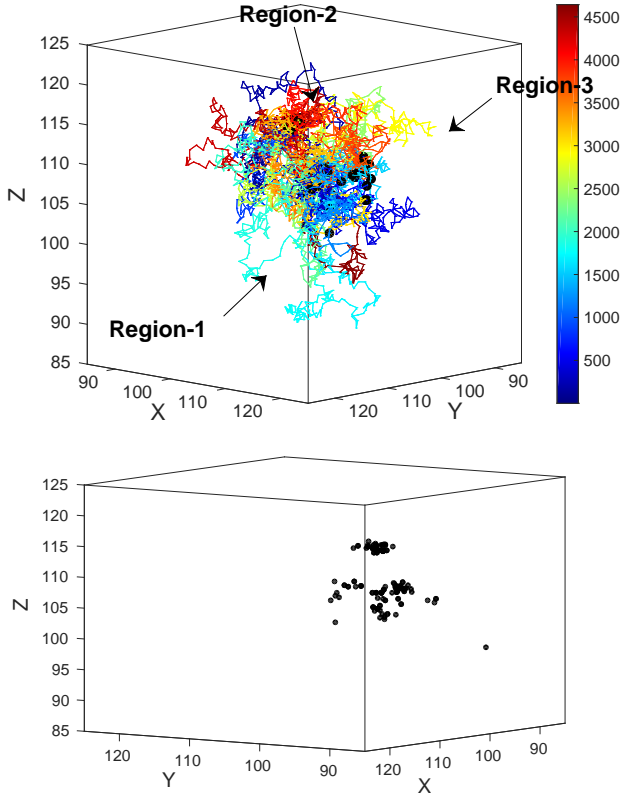


FIG. 18. Representative snapshot from our simulation of DNA-polymer with BC-2 is shown in the top figure. The colorbar on the right shows the color which is used to represent the monomers numbered from 1 to 4642. The black circles show the positions of CLs. The bottom figure shows the position of CLs in space where we have removed the other monomers for better visualization. The coordinates are the same as used for the snapshot above.

Moreover, the figure confirms the kind of conformations expected from the colormaps of angular correlation shown in Fig.17(a) and (b). For example the section marked Region-1 representing monomers around 1750 (segment index 30) is diametrically opposite Region-3 with monomer index 2990 (segment index 50). In Fig.17 (a) we see the pixel corresponding to segment indices (30,50) are black. The Region-2 represents monomer numbered around 4100, segment index 71. We can see the pixels corresponding to segment indices (30,71) is yellow whereas pixels for (50,71) is white. The bottom figure shows the CL distribution in space: only one of monomers out of the pair which constitute a CL has been plotted. It is interesting to observe that the CLs are clumped together in space in about four aggregates. We believe that this helps in the meso-scale organization of the chain as multiple segments of the chain are pulled towards the globule's center with multiple loops on the periphery of the globule. The peripheral loops can lead to relatively large fluctuations in the values of I_1/I_3 as seen in Fig.3.

IV. DISCUSSION

The primary and new conclusion of our study is that for a DNA-ring polymer, if a particular sets of monomers are held together by a suitable proteins (multiple cross-links at specific points in our model polymer) it leads to a particular structure and organization of the DNA chain which is reminiscent of the fractal globule structure [2, 25]. Thus we can claim that sets of CLs at specific locations along the chain are not at random positions along the contour. Randomly chosen location of CLs also result in large scale organization of a polymer, but the nature of organization is different, which is in variance with [18, 19]. Of course, the DNA polymer undergoes local conformational fluctuations due to the thermal energy but overall the structure is maintained in a statistical sense. We can deduce the presence of distinctive meso-scale organization of DNA from the calculation of three quantities: (a) radial distribution of segments, (b) positional correlations between segments and (c) angular correlations between segments. Thus we have much more detailed information of organization of different segments than can be obtained from pair correlation function. We have only a rudimentary understanding about the position of cross-links which allow a chain to maintain structure. We have given a possible argument of how structure is obtained, but a full understanding and systematic methodology of the choice of CL-positions can be developed only in future, when we have access to larger number of contact maps of many DNAs.

We acknowledge the use of computational facilities provided by DBT Alliance, project numbers IA/I/12/1/500529, IA/I/11/2500290, to C. Assisi, S. Nadkarni, M.S. Madhusudhan. We also acknowledge the use of a cluster bought using DST-SERB grant no. EMR/2015/000018 to A. Chatterji. A.C acknowledges funding support by the Department of Science and Technology (DST, Govt. of India) under the DST Nanomission Thematic Unit Program.

V. APPENDIX: GENERATION OF CONTACT FREQUENCY MAP

In the field of bioinformatics, a sequence database is a biological database which is a collection of computerized nucleic acid sequences. Paired-end sequencing allows researchers to sequence both ends of a DNA-fragment to generate high-quality, alignable sequence data. Paired-end sequencing facilitates detection of genomic reorganization and repetitive sequence elements.

In a paired end-sequencing run, the distance between the alignments of the two fragments is the length of the DNA fragment being sequenced. Aligners (software tools) use this information to better align reads when faced with a read that align to multiple regions such as those that may lie in a repeat region. To avoid this behavior, the reads are aligned in single end mode while

keeping track of the pairs. We have employed the BWA [44] aligner to align reads as it has best sensitivity among short read aligners.

The aligned reads are then binned at the desired resolution (or the minimum distance between restriction sites). A 2D matrix with the required number of bins is initialized. A large fraction of the reads in a 3C library were from fragments that were not cross-linked and fall into the same bin or bins adjacent to each other. These read pairs were filtered out. The counter in the bin with the coordinates indicated by the alignment of each read in the pair is incremented for all the remaining reads. The filled matrix gives the total number of contacts between different parts of the genome and the resulting matrix is called the contact map.

To be able to compare between different runs, the contact map is normalized so that effect of varying number of sequenced reads is accounted for. Each sum of the number of contacts in each row and column in the matrix were normalized to 1. This provides a normalized contact map, which can now be used to elucidate the 3D structure of the genome and compare changes across

different conditions.

Escherichia coli (*E. coli*) strain K12-MG1622 were obtained from German collection of microorganisms and cell cultures at Leibniz institute (DSMZ).

The aligned reads were then binned at the desired resolution (or the minimum distance between restriction sites). A 2D matrix with the required number of bins was initialized. A large fraction of the reads in a 3C library were from fragments that were not cross-linked and fall into the same bin or bins adjacent to each other. These read pairs were filtered out. The counter in the bin with the coordinates indicated by the alignment of each read in the pair is incremented for all the remaining reads. The filled matrix gives the total number of contacts between different parts of the genome and the resulting matrix is called the contact map. To be able to compare between different runs, the contact map were normalized so that effect of varying number of sequenced reads is accounted for. Each sum of the number of contacts in each row and column in the matrix were normalized to 1. This provides a normalized contact map, which can now be used to elucidate the 3D structure of the genome.

-
- [1] Dekker, M.-R. MA, and M. LA, *Nat Rev Genet* **14**, 390 (2013).
 - [2] Lieberman-Aiden, N. L. van Berkum, L. Williams, M. Imakaev, I. A. T. Ragozy, A. Telling, B. R. Lajoie, P. J. Sabo, M. O. Dorschner, B. B. R. Sandstrom, M. A. Bender, J. S. M. Groudine, A. Gnirke, L. A. Mirny, and J. D. E. S. Lander, *Science* **326**, 289 (2009).
 - [3] J. Dekker and L. Mirny, *Cell* **164**, 1110 (2016).
 - [4] W. A. Bickmore and B. van Steensel, *Cell* **152**, 1270 (2013.).
 - [5] T. Sexton, E. Yaffe, E. Kenigsberg, F. Bantignies, B. Leblanc, M. Hoichman, H. Parrinello, A. Tanay, and G. Cavalli, *Cell* **148**, 458 (2012).
 - [6] J. R. Dixon, S. Selvaraj, F. Yue, A. Kim, M. H. Y. Li, Y. Shen, J. S. Liu, and B. Ren, *Nature* **485**, 376 (2012).
 - [7] L. A. M. Maxim V. Imakaev, Geoffrey Fudenberg, *FEBS Letters* **589**, 3031 (2015).
 - [8] D. Chaudhuri and B. Mulder, *Phys. Rev. E* **83** (2011), 10.1103/PhysRevE.83.031803.
 - [9] D. Chaudhuri and B. M. Mulder, *Phys. Rev. Lett* **108** (2012), 10.1103/PhysRevLett.108.268305.
 - [10] K. K. Jonathan D Halverson, Jan Smrek and A. Y. Grosberg, *Reports on Progress in Physics* **77** (2014.).
 - [11] A. Y. Grosberg, *Biophysical Journal* **110**, 21332135 (2016).
 - [12] D. W. H. Andreas Hofmann, *FEBS Letters* **589**, 2958 (2015).
 - [13] N. Ramakrishnan, K. Gowrishankar, L. Kuttippurathu, P. B. S. Kumar, and M. Rao, "Active remodeling of chromatin and implications for in-vivo folding," (2015), arXiv:1510.04157.
 - [14] G. Fudenberg, M. Imakaev, C. Lu, A. Goloborodko, N. Abdennur, and L. A. Mirny, *Cell Reports* **15**, 2038 (2016).
 - [15] A. Rosa and R. Everaers, *PLOS Computational Biology* **4**:e1000153 (2008), 10.1371/journal.pcbi.1000153.
 - [16] A. Pombo and M. Nicodemi, *Current Opinion in Cell Biology*, **28** (2014.).
 - [17] A. M. Chiariello, C. Annunziatella, S. Bianco, A. Esposito, and M. Nicodemi, *Nature Scientific Reports* **6** (2016.).
 - [18] R. Kalhor, H. Tjong, N. Jayathilaka, F. Alber, and L. Chen, *Nature Biotechnology* **30**, 90 (2012).
 - [19] H. Tjong, K. Gong, Chen, L., and F. Alber, *Genome Res.* **22**, 1295 (2012).
 - [20] B. V. S. Iyer and G. Arya, *Phys. Rev. E* **86** (2012), 10.1103/PhysRevE.86.011911.
 - [21] T. Misteli, *Cell* **128**, 787 (2007.).
 - [22] L. TB, I. MV, M. LA, and L. MT., *Science* **342**, 731 (2013).
 - [23] C. C, G. RS, J. MB, J. DJ, and O. JM, *Nucleic Acids Res.* **41**, 6058 (2013).
 - [24] J. E. Phillips-Cremins, M. E. Sauria, A. Sanyal, T. I. Gerasimova, B. R. Lajoie, J. S. Bell, C.-T. Ong, T. A. Hookway, C. Guo, Y. Sun, M. J. Bland, W. Wagstaff, S. Dalton, T. C. McDevitt, R. Sen, J. Dekker, J. Taylor, and V. G. Corces., *Cell* **153**, 1281 (2013.).
 - [25] M. V. Imakaev, K. M. Tchourine, S. K. Nechaev, and L. A. Mirny, *Soft Matter* **11**, 665 (2015).
 - [26] L. A. Mirny, *Chromosome Res* **19**, 37 (2011.).
 - [27] A. Vologodskii, *Nucleic Acids Res.* **37**, 3125 (2009).
 - [28] R. K. Sachs, G. van den Engh, B. Trask, H. Yokota, , and J. E. Hearst., *PNAS U.S.A.* **92**, 2710 (1995.).
 - [29] D. Marenduzzo, C. Micheletti, and P. R. Cook, *Biophysical Journal* **90**, 3712 (2006.).
 - [30] M. Bohn and D. W. Heermann, *PLoS ONE* 10.1371/journal.pone.0012218., e12218.
 - [31] D. Jost, P. Carrivain, G. Cavalli, and C. Vaillant, *Nucl Acids Res* **42**, 9553 (2014).
 - [32] M. Barbieri, M. Chotalia, J. Fraser, L.-M. Lav-

- itas, J. Dostie, A. Pombo, and M. Nicodemi, PNAS U.S.A. **109**, 16173 (2012).
- [33] L. Giorgetti, R. Galupa, E. P. Nora, T. Piolot, F. Lam, J. Dekker, G. Tiana, and E. Heard, Cell **157** (2014), 10.1016/j.cell.2014.03.025.
 - [34] G. Fudenberg, M. Imakaev, C. Lu, A. Goloborodko, and N. Abdennur, Cell Reports **15**, 2038 (2016).
 - [35] A. Goloborodko, J. F. Marko, and L. A. Mirny, Biophysical Journal **110**, 2162 (2016).
 - [36] G. AY and K. AR, *Statistical physics of macromolecules* (AIP, New York., 1994).
 - [37] G. PGD, *Scaling concepts in polymer physics* (Cornell University Press, Ithaca., 1979).
 - [38] R. M and C. RH, *Polymer physics* (Oxford University Press, Oxford., 2003).
 - [39] J. T. Rob Phillips, Jane Kondev, *Physical Biology of the Cell* (Garland Science., 2008).
 - [40] J. Mateos-Langerak, M. Bohn, W. de Leeuw, O. Giromus, E. M. M. Manders, P. J. Verschure, M. H. G. Indemans, H. J. Gierman, D. W. Heermann, R. van Driel, and S. Goetze, PNAS U.S.A. **106**, 3812 (2009).
 - [41] M. Rousseau, J. Fraser, M. A. Ferriaiuolo, J. Dostie, and M. Blanchette, BMC Bioinformatics **12** (2011), 10.1186/1471-2105-12-414.
 - [42] D. Ba, A. Sanyal, B. R. Lajoie, E. Capriotti, M. Byron, J. B. Lawrence, J. Dekker, and M. A. Marti-Renom, Nature Structural & Molecular Biology **18**, 107 (2011).
 - [43] M. Muller, J. P. Wittmer, and M. E. Cates, Physical Review E **53**, 5063 (1996).
 - [44] H. Li and R. Durbin, Bioinformatics, **26**, 589 (2010.).

Supplementary Materials

VI. LIST OF CROSS-LINKED MONOMERS IN OUR SIMULATIONS.

In the following table, we list the monomers which are cross-linked to model the constraints for the DNA of bacteria *E. Coli*. Note that for random cross links (CL) set-1 and set-2 (RC-1, RC-2) we have fewer number of CLs, as there are fewer *effective* CLs in the list of CLs.

In particular while counting the number of independent CLs, one should pay special attention to the points listed below. As a consequence, 47 CLs of BC-1 should be counted as only 27 independent CLs. Hence, we use just 26 CLs in RC-1, when we compare organization of

RC-1 and BC-1. Correspondingly, we have just 82 CLs in RC-2, instead of 158 in BC-2.

- The rows corresponding to independent cross-links of set BC-1 are marked by *, one can observe that the next row of CLs are adjacent to the monomers marked just previously by *. These cannot be counted as independent CLs.
- The rows marked by + is not a independent CL at all, monomers 733 and 735 are trivially close to each other by virtue of their position along the contour.

This table has been generated by analysis of raw data obtained from C. Cagliero et. al., Nucleic Acids Res, **41**, 6058-6071 (2013).

-	BC-1		RC-1		BC-2		RC-2	
Serial no.	Monomer index-1	Monomer index-2	Monomer index-1	Monomer index-2	Monomer Index-1	Monomer Index-2	Monomer Index-1	Monomer Index-2
1	1*	4642	1	4642	1	4642	1	4642
2	16*	2515	3739	4531	16	2515	3739	4531
3	17	2516	3011	1610	17	2516	3011	1610
4	20*	1051	2582	4367	20	1051	2582	4367
5	224*	2731	3370	1680	20	3584	3370	1680
6	225	2731	556	2622	21	1050	556	2622
7	226	2730	1676	1426	21	3584	1676	1426
8	226*	3428	998	2741	224	2731	998	2741
9	227	2728	474	2233	224	3429	474	2233
10	227	2729	2522	533	224	4208	2522	533
11	228	2727	1967	2490	224	4209	1967	2490
12	228	2728	2536	616	225	2730	2536	616
13	229*	2727	769	4614	225	2731	769	4614
14	271*	4509	2	2023	226	2729	2	2023
15	272	4508	3494	2484	226	2730	3494	2484
16	275*	1300	2534	1365	226	3427	2534	1365
17	280*	1051	3053	2256	226	3428	3053	2256
18	291*	1051	3779	2647	226	4038	3779	2647
19	316*	393	4199	4452	226	4169	4199	4452
20	317*	2172	2839	1309	227	2728	2839	1309
21	382*	1469	1385	449	227	2729	1385	449
22	383	1469	4398	371	228	2727	4398	371
23	527*	1529	522	1434	228	2728	522	1434
24	575*	1301	3676	320	228	3946	3676	320
25	609*	2515	178	4317	229	2727	178	4317
26	730*	3763	3220	515	229	3424	3220	515
27	731	3764	527	2992	229	3947	527	2992
28	732	3765	-	-	229	3948	2391	1402
29	733 ⁺	735	-	-	229	4172	284	4086
30	733*	3766	-	-	229	4213	4311	2243
31	1301*	3132	-	-	229	4214	283	1687
32	1433*	1635	-	-	271	4509	1599	2420
33	1434	1634	-	-	272	1471	4445	3365
34	1533*	3626	-	-	272	4508	1523	739
35	1571*	3667	-	-	274	1301	2721	113
36	1572	3668	-	-	275	1300	1371	4360
37	2728*	3945	-	-	275	1301	4137	2593
38	2729	3945	-	-	275	3130	1026	2807
39	2730	3943	-	-	276	2291	3007	2767
40	3429*	3942	-	-	276	3130	1576	1282
41	3471*	4177	-	-	276	3367	3041	3010
42	3620*	3763	-	-	280	292	2558	2709

43	3620	3764	-	-	280	1050	2156	3872
44	3621	3764	-	-	280	1051	945	4229
45	3622	3765	-	-	291	1051	4465	2873
46	3622	3766	-	-	291	2760	1943	4488
47	3623*	3766	-	-	315	393	4286	881
48	-	-	-	-	316	391	3282	3882
49	-	-	-	-	316	392	3555	2445
50	-	-	-	-	316	393	1196	40
51	-	-	-	-	317	392	1997	3918
52	-	-	-	-	317	568	4178	1595
53	-	-	-	-	317	569	678	3768
54	-	-	-	-	317	1094	3519	164
55	-	-	-	-	317	1095	2979	4115
56	-	-	-	-	317	2172	2871	3747
57	-	-	-	-	382	1469	3930	4263
58	-	-	-	-	383	1468	2787	2654
59	-	-	-	-	383	1469	1101	831
60	-	-	-	-	393	567	2785	1485
61	-	-	-	-	393	1096	3477	1069
62	-	-	-	-	393	2171	2345	795
63	-	-	-	-	526	1529	4037	3848
64	-	-	-	-	527	1529	395	1040
65	-	-	-	-	527	1530	328	930
66	-	-	-	-	575	1301	1926	2551
67	-	-	-	-	576	3130	4440	1484
68	-	-	-	-	576	3367	3799	4456
69	-	-	-	-	581	1636	4129	837
70	-	-	-	-	581	1637	1500	1352
71	-	-	-	-	582	1636	3197	947
72	-	-	-	-	608	2515	263	3435
73	-	-	-	-	609	2515	2272	277
74	-	-	-	-	688	1301	4276	702
75	-	-	-	-	730	3763	3405	978
76	-	-	-	-	731	3763	388	3658
77	-	-	-	-	731	3764	2796	1022
78	-	-	-	-	732	3621	3411	1122
79	-	-	-	-	732	3764	861	2185
80	-	-	-	-	732	3765	3564	1606
81	-	-	-	-	733	735	1860	1447
82	-	-	-	-	733	3623	904	3577
83	-	-	-	-	733	3765	-	-
84	-	-	-	-	733	3766	-	-
85	-	-	-	-	734	3765	-	-
86	-	-	-	-	734	3766	-	-
87	-	-	-	-	738	1533	-	-
88	-	-	-	-	738	3626	-	-
89	-	-	-	-	782	2522	-	-
90	-	-	-	-	1051	3585	-	-
91	-	-	-	-	1208	1210	-	-
92	-	-	-	-	1269	1271	-	-
93	-	-	-	-	1301	1398	-	-
94	-	-	-	-	1301	2102	-	-
95	-	-	-	-	1301	2289	-	-
96	-	-	-	-	1301	3132	-	-
97	-	-	-	-	1301	3366	-	-
98	-	-	-	-	1301	3652	-	-
99	-	-	-	-	1397	2573	-	-
100	-	-	-	-	1397	3118	-	-
101	-	-	-	-	1433	1635	-	-
102	-	-	-	-	1434	1634	-	-
103	-	-	-	-	1435	1633	-	-
104	-	-	-	-	1469	2071	-	-
105	-	-	-	-	1470	2071	-	-
106	-	-	-	-	1470	2998	-	-

107	-	-	-	-	1470	3186	-	-
108	-	-	-	-	1470	4498	-	-
109	-	-	-	-	1470	4508	-	-
110	-	-	-	-	1470	4509	-	-
111	-	-	-	-	1471	4508	-	-
112	-	-	-	-	1533	3625	-	-
113	-	-	-	-	1533	3626	-	-
114	-	-	-	-	1571	3667	-	-
115	-	-	-	-	1572	3667	-	-
116	-	-	-	-	1572	3668	-	-
117	-	-	-	-	2726	4172	-	-
118	-	-	-	-	2727	4172	-	-
119	-	-	-	-	2728	3945	-	-
120	-	-	-	-	2728	4039	-	-
121	-	-	-	-	2728	4171	-	-
122	-	-	-	-	2729	3945	-	-
123	-	-	-	-	2729	4038	-	-
124	-	-	-	-	2730	3943	-	-
125	-	-	-	-	2730	4038	-	-
126	-	-	-	-	2731	3942	-	-
127	-	-	-	-	2731	4036	-	-
128	-	-	-	-	2732	3942	-	-
129	-	-	-	-	3424	4172	-	-
130	-	-	-	-	3426	3945	-	-
131	-	-	-	-	3426	4156	-	-
132	-	-	-	-	3427	3944	-	-
133	-	-	-	-	3427	4038	-	-
134	-	-	-	-	3428	3943	-	-
135	-	-	-	-	3428	3944	-	-
136	-	-	-	-	3429	3942	-	-
137	-	-	-	-	3471	4177	-	-
138	-	-	-	-	3472	4176	-	-
139	-	-	-	-	3472	4177	-	-
140	-	-	-	-	3619	3763	-	-
141	-	-	-	-	3620	3763	-	-
142	-	-	-	-	3620	3764	-	-
143	-	-	-	-	3621	3764	-	-
144	-	-	-	-	3621	3765	-	-
145	-	-	-	-	3622	3765	-	-
146	-	-	-	-	3622	3766	-	-
147	-	-	-	-	3623	3766	-	-
148	-	-	-	-	3623	3768	-	-
149	-	-	-	-	3942	4167	-	-
150	-	-	-	-	3942	4209	-	-
151	-	-	-	-	3943	4038	-	-
152	-	-	-	-	3944	4038	-	-
153	-	-	-	-	3944	4169	-	-
154	-	-	-	-	3944	4210	-	-
155	-	-	-	-	4036	4167	-	-
156	-	-	-	-	4036	4209	-	-
157	-	-	-	-	4037	4443	-	-
158	-	-	-	-	4041	4214	-	-
159	-	-	-	-	4172	4214	-	-

TABLE I: Table shows the list of pair of monomers which constitute the CLs for *E. Coli*, these CLs are used as an input to the simulation by constraining these monomers to be at a distance a from each other. The first monomer with label 1 and the last monomer labelled 4642 are linked together because the DNA is a ring polymer.

VII. RADIAL LOCATION OF CLS AND SEGMENT'S CM OF *E. COLI*.

In the main manuscript, we show the radial organization of different CLs and segment-CMs in Figs.6 and

Fig.7, respectively for BC-2 and compare it with the DNA-polymer with CLs corresponding to RC-2, which has the same number of effective CLs as in BC-2. In the

following, we give analogous plots with BC-1 and RC-1.

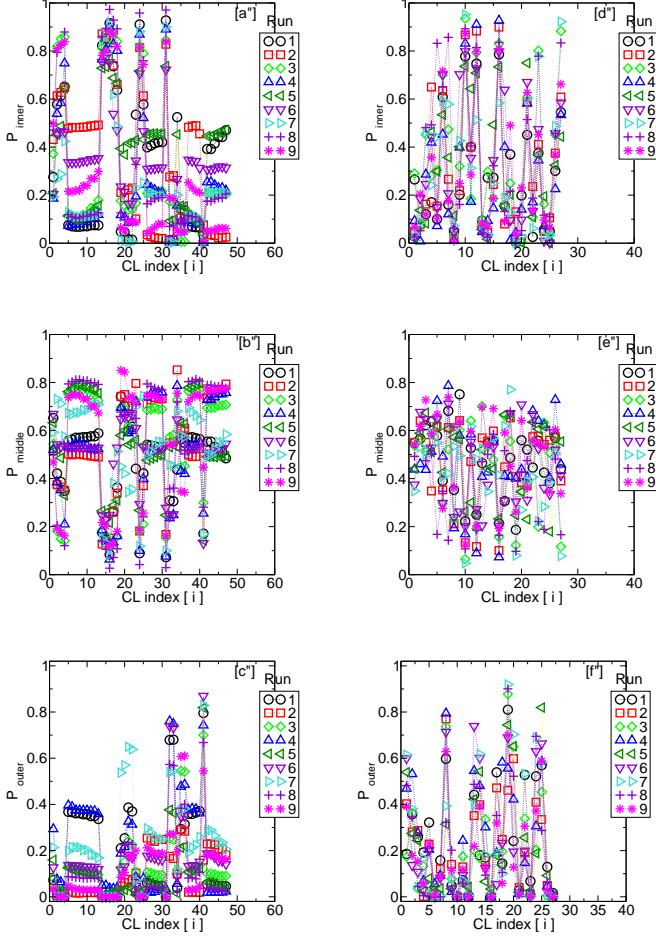


FIG. 19. Data for bacteria *E. Coli* with no. of CLs = BC-1 : Subplots (a''), (b'') and (c'') show the probabilities of CLs to be found in the inner, middle and outer region of DNA globule. The x-axis is segment index, different lines are from independent runs starting from different initial conditions. Subplots (d''), (e''), (f'') are for RC-1. Each segment has 58 monomers, the dna-polymer has around 80 segments.

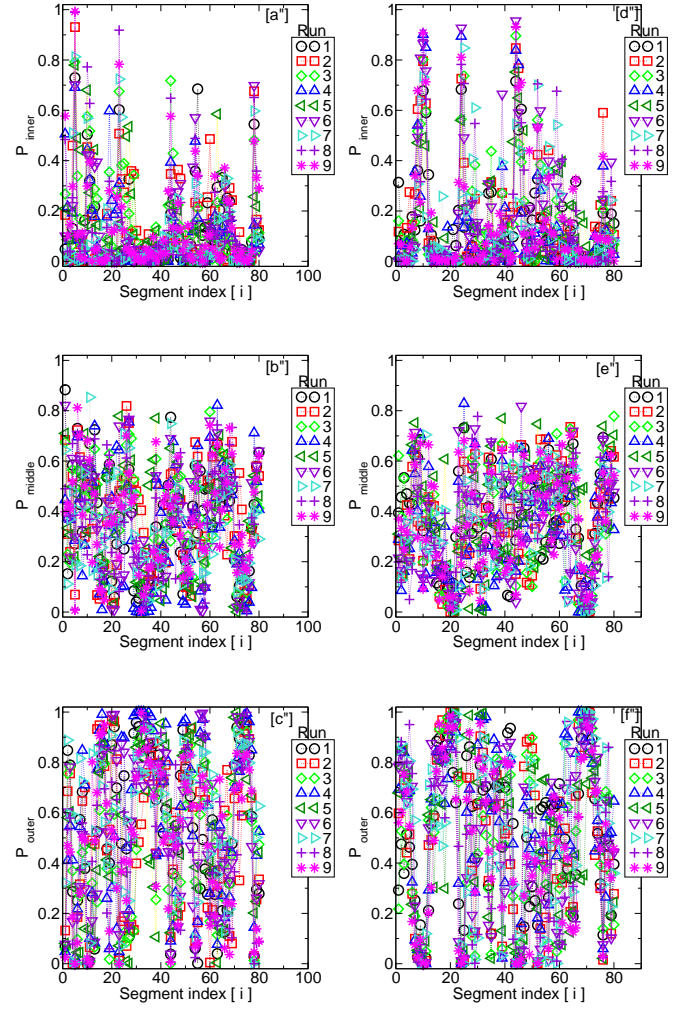


FIG. 20. Data for bacteria *E. Coli* with no. of CLs = BC-1 : Subplots (a'), (b') and (c') show the probabilities of center of mass of polymer segments to be found in the inner, middle and outer region of polymer globule. The x-axis is segment index, different lines are from independent runs starting from different initial conditions. Subplots (d'), (e'), (f') are for RC-1. Each segment has 58 monomers, the dna-polymer has around 80 segments.

VIII. COLOR-MAPS FOR POSITIONAL CORRELATIONS

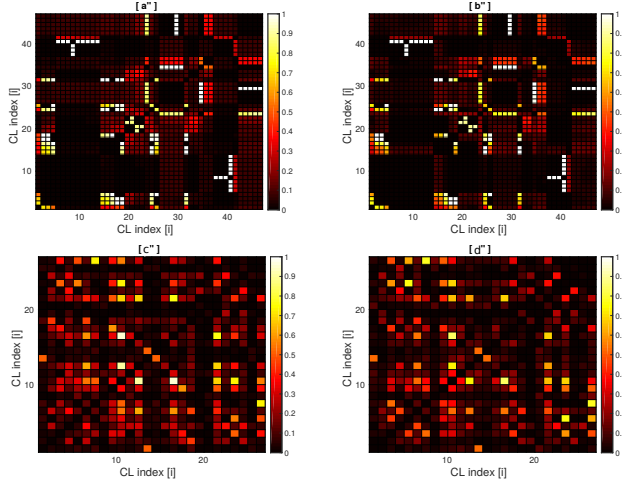


FIG. 21. Colormaps show the probability to find CLs i and CLs j within a distance of 5σ . The colormaps (a''), (b'') and (c'') and (d'') are from two additional independent runs for BC-1 and RC-1, respectively.

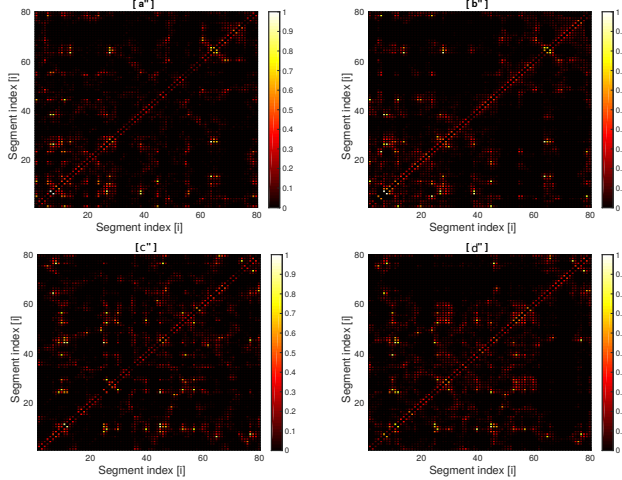


FIG. 22. Colormaps show the probability of center of mass of the segments (i) (58 monomer each) to be found within a distance 5σ of other segment's center of mass. The colormaps (a''), (b'') and (c'') and (d'') are from two additional independent runs for BC-1 and RC-1, respectively.

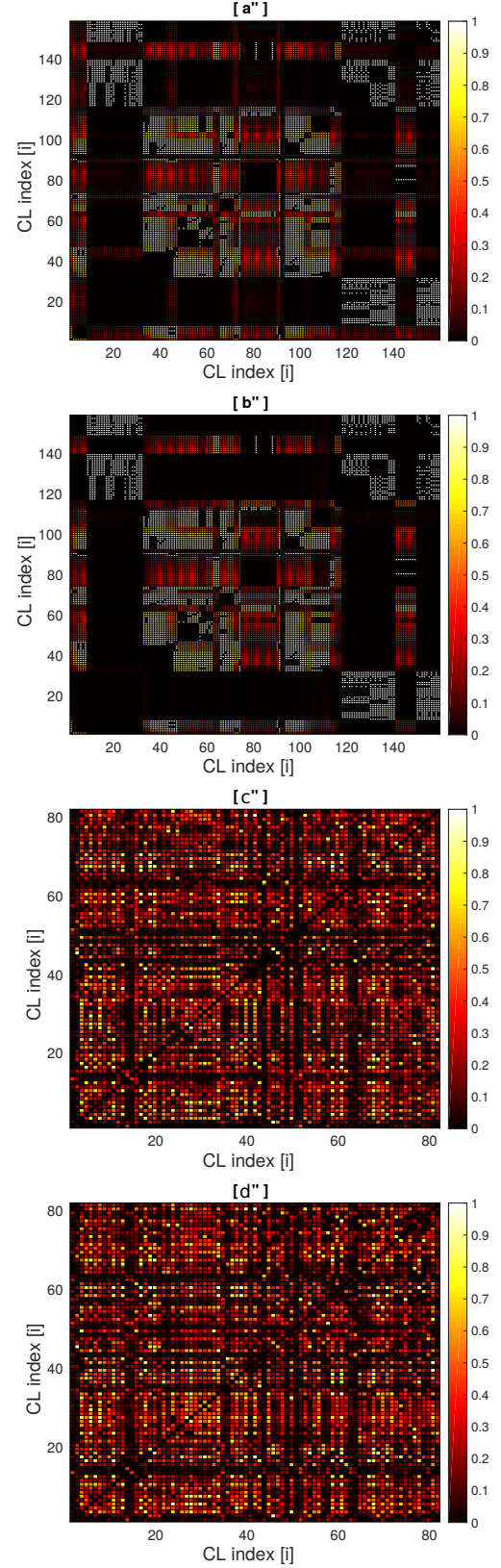


FIG. 23. Colormaps show the probability to find CLs i and CLs j within a distance of 5σ . The colormaps (a''), (b'') and (c'') and (d'') are from two additional independent runs for BC-2 and RC-2, respectively.

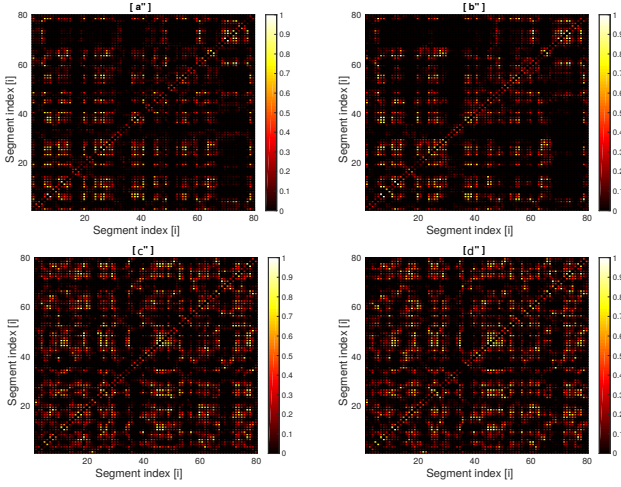


FIG. 24. Colormaps show the probability of center of mass of the segments (i) (58 monomer each) to be found within a distance 5σ of other segment's center of mass. The colormaps (a''), (b'') and (c'') and (d'') are from two additional independent runs for BC-2 and RC-2, respectively.

IX. COLOR-MAPS FOR ANGULAR CORRELATIONS

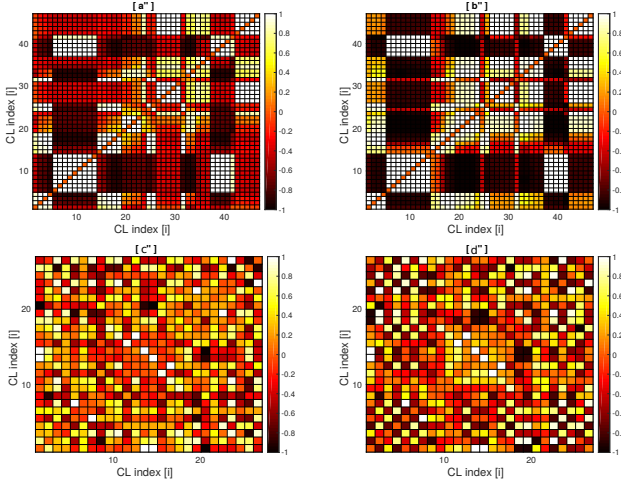


FIG. 25. Colormaps show the angular positions of different CL with respect to each other. The colormaps (a''), (b'') and (c'') and (d'') are from two additional independent runs for BC-1 and RC-1, respectively.

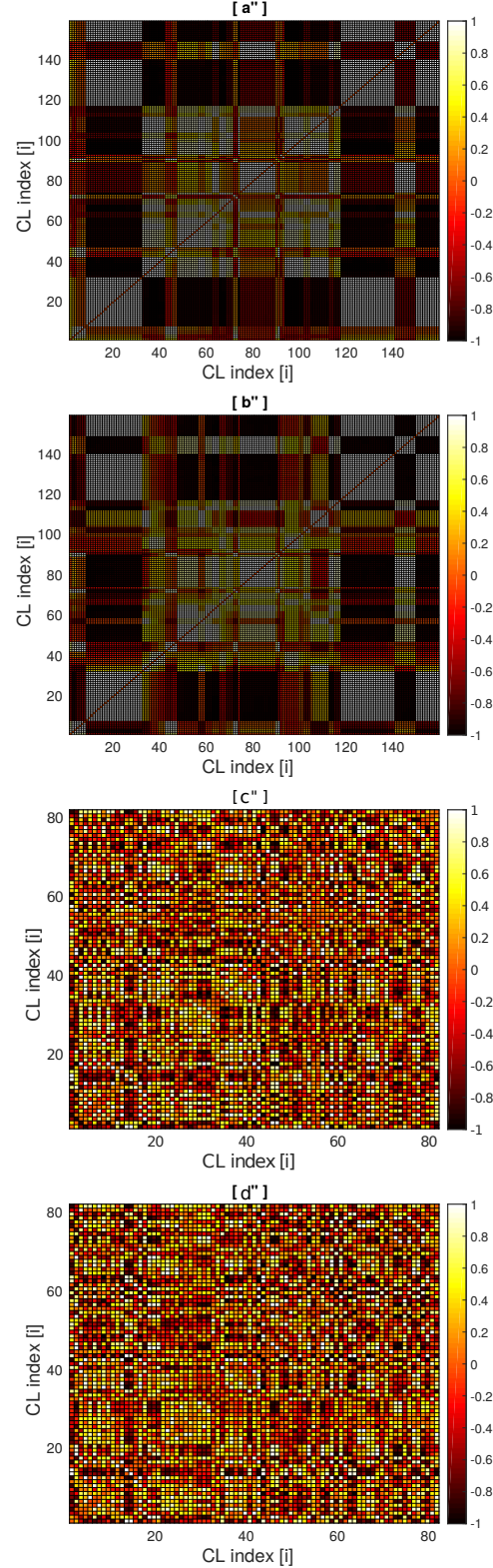


FIG. 26. Colormaps show the angular positions of different CL with respect to each other. The colormaps (a''), (b'') and (c'') and (d'') are from two additional independent runs for BC-2 and RC-2, respectively.

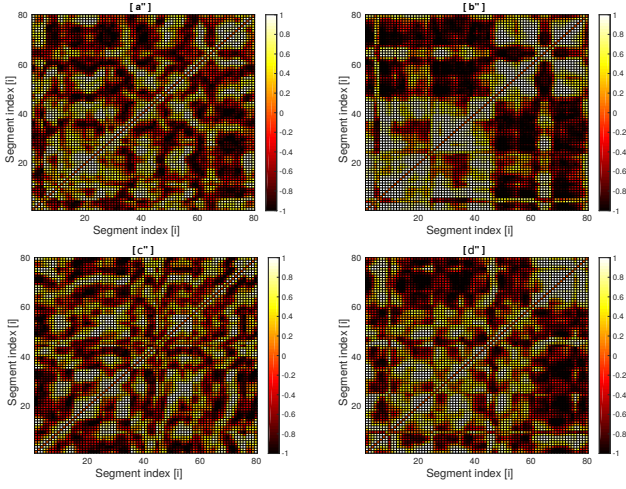


FIG. 27. Colormaps show the angular positions of center of mass of the different segments with respect to each other. The colormaps (a''), (b'') and (c'') and (d'') are from two additional independent runs for BC-1 and RC-1, respectively.

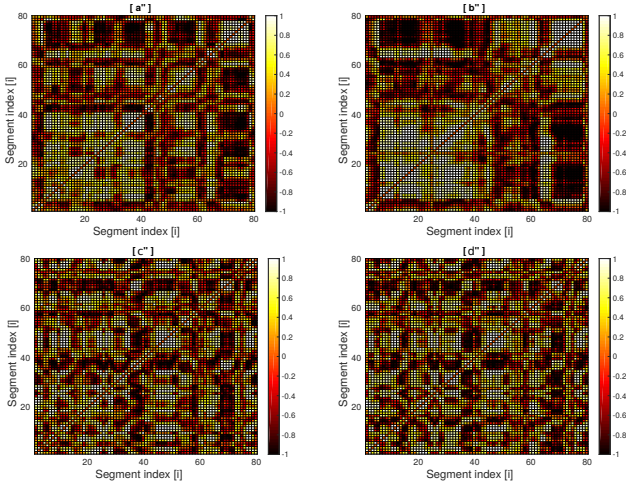


FIG. 28. Colormaps show the angular positions of center of mass of the different segments with respect to each other. The colormaps (a''), (b'') and (c'') and (d'') are from two additional independent runs for BC-2 and RC-2, respectively.